Evaluation of biogeochemical models performance and recommendation on observing system design using an unsupervised machine learning algorithm, BGC-Argo floats and assessment metrics

Alexandre Mignot[1], Hervé Claustre[2,3], Gianpiero Cossarini[4], Fabrizio D'Ortenzio[2,3], Elodie Gutknecht[1], Julien Lamouroux[1], Paolo Lazzari[4], Coralie Perruche[1], Stefano Salon[4], Raphaelle Sauzède[3], Vincent Taillandier[2,3], Anna Teruzzi[4]

[1]Mercator Océan International, Toulouse, France

[2]Laboratoire d'Océanographie de Villefranche-sur-Mer, Villefranche-sur-Mer, CNRS and Sorbonne Université, 06230 Villefranche-sur-Mer, France

[3]Institut de la Mer de Villefranche, CNRS and Sorbonne Université, 06230 Villefranche-sur-Mer, France

[4]National Institute of Oceanography and Applied Geophysics - OGS, Trieste, Italy

Numerical models of ocean biogeochemistry are becoming major tools to detect and predict the impact of climate change on marine resources and monitor ocean health. However, the assessment of biogeochemical models is becoming increasingly challenging due to the continuous improvement in model structure and spatial resolution. Here, we propose a new method to inform about the model predictive skill in a concise way. The method is based on the conjoint use of a K-means clustering technique -- an unsupervised machine learning algorithm, assessment metrics and BGC-Argo observations. The K-means algorithm and the assessment metrics reduce the number of model data points to be evaluated. The metrics evaluate either the model state accuracy or the skill of the model in capturing emergent properties, such as the Deep Chlorophyll Maximums and Oxygen Minimum Zones. The use of BGC-Argo observations as the single evaluation data set ensure the accuracy of the data as it is an homogenous data set with strict sampling methodologies and data quality control procedures. The method is applied to the Copernicus Marine Service global forecasting system. The model performance is evaluated using the model efficiency statistical score that compare the model-observations misfit with the variability of the observations, and thus objectively quantifies whether the model outperforms the BGC-Argo climatology. We show

Style Definition: Heading 1: Don't keep lines together

Style Definition: Normal (Web): Space Before: Auto, After: Auto

Style Definition: List Paragraph: Font: (Default) Times New Roman

Deleted: Using BGC-Argo floats for the assessment

Deleted: marine

Deleted: : a case study with CMEMS global forecast

Deleted: a

Deleted: tool

Deleted: Classically, the validation of such models relies on comparison with surface quantities from satellite (such as chlorophyll-*a* concentrations), climatologies, or sparse *in situ* data (such as cruises observations, and permanent fixed oceanic stations).

Deleted: these datasets are not fully suitable to assess how models represent many climate-relevant biogeochemical processes. These limitations now begin to be overcome with the availability of a large number of vertical profiles of light, pH, oxygen, nitrate, chlorophyll-*a* concentrations and particulate backscattering acquired by the Biogeochemical-Argo (BGC-Argo) floats network. Additionally, other key biogeochemical variables such as dissolved inorganic carbon and alkalinity, not measured by floats, can be predicted by machine learning-based methods applied to float oxygen concentrations. Here, we demonstrate the use of the global¶ array of BGC-Argo floats for

Formatted: Font: Times New Roman

Deleted: through a¶ concise evaluation of the Copernicus Marine Environment Marine Service (CMEMS) global forecasting system. We first detail the handling of the BGC-Argo data set for

Deleted: assessment purposes, then we present 22

Deleted: to quantify

Deleted: consistency

Deleted: BGC

Deleted: simulations with respect to BGC-Argo

Deleted: .

Deleted: (DCMs) or

Deleted: (OMZs). These metrics are associated with

Deleted: air-sea CO2 flux,

Deleted: biological

that, overall, the model surpass the BGC-Argo climatology in predicting pH, dissolved inorganic carbon, alkalinity and oxygen in the mesopelagic and the mixed layers, nitrate, silicate and phosphate in the mesopelagic layer. We provide suggestions to reduce the model-data misfit for phosphate, silicate, pH and the partial pressure of CO_2 in the mixed layer, chlorophyll-a related and particulate organic carbon metrics, and Oxygen Minimum Zones. The method proposed here is also helpful to inform about the design of the BGC-Argo network. In particular, the regions where BGC-Argo observations should be enhanced to improve the model accuracy through the assimilation of BGC-Argo data or process-oriented assessment studies. We strongly recommend to enhance the Arctic region, which is critically under sampled and where the model is constantly outperformed by the BGC-Argo climatology. BGC-Argo observations should also be reinforced in the Equatorial region and in the Southern Oceans, two regions where the model predictions barely exceed the BGC-Argo climatology. Our results illustrate how the synergic use of modeling and BGC-Argo data can both inform about the performance of models and the design of observing systems.

1. Introduction

Since pre-industrial times, the ocean has taken ~26 % of the total anthropogenic CO_2 emission (Friedlingstein et al., 2022) leading to dramatic change in the ocean's biogeochemical (BGC) cycles, such as ocean acidification (Iida et al., 2020). Moreover, deoxygenation (Breitburg et al., 2018) and change in the biological carbon pump are now manifesting globally (Capuzzo et al., 2018; Osman et al., 2019; Roxy et al., 2016). Together with plastic pollution (Eriksen et al., 2014) and an increase in fisheries pressure (Crowder et al., 2008), major changes are therefore occurring in marine ecosystems at the global scale. In order to contextualize monitoring of ongoing changes, derive climate projections and develop better mitigation strategies, realistic numerical simulations of the oceans' BGC state are required.

Numerical models of ocean biogeochemistry represent a prime tool to address these issues because they produce three dimensional estimates of a large number of chemical and biological variables that are dynamically consistent with the ocean circulation (Fennel et al., 2019). They can assess past and current states of the BGC ocean, produce short-term to

Deleted: pump, and the oceanic pH and oxygen levels. We also suggest four diagnostic plots for displaying such

Deleted: .

Deleted: Since pre-industrial times, the ocean had taken up ~36 % of the CO_2 emitted by the combustion of fossil fuel (Friedlingstein et al., 2019) leading to dramatic change in the ocean's biogeochemical (BGC) cycles, such as ocean acidification (Iida et al., 2020). Moreover, deoxygenation (Breitburg et al., 2018) and change in the biological carbon pump are now manifesting on a global scale (Capuzzo et al., 2018; Osman et al., 2019; Roxy et al., 2016). Together with plastic pollution (Eriksen et al., 2014) and an increase in fisheries pressure (Crowder et al., 2008), major changes are therefore occurring in marine ecosystems at the global scale. In order to monitor these ongoing changes, derive climate projections and develop better mitigation strategies, realistic numerical simulations of the oceans' BGC state are required. ¶
¶
Numerical models of ocean biogeochemistry represent a prime tool to address these issues because they produce three dimensional estimates of a large number of chemical and biological variables that are dynamically consistent with the ocean circulation (Fennel et al., 2019). They can assess past and current states of the biogeochemical ocean, produce short-term to seasonal forecasts as well as climate projections. However, these models are far from being flawless, mostly because there are still huge knowledge gaps in the understanding of key biogeochemical processes and, as a result, the mathematical functions that describe BGC fluxes and ecosystems dynamics are too simplistic (Schartau et al., 2017). For instance, most models do not include a radiative component for the penetration of solar radiation in the ocean. It has been nevertheless shown that coupling such a component with a BGC model improves the representation of the dynamics of phytoplankton in the lower euphotic zone (Dutkiewicz et al., 2015). Additionally, the parameterisation of the mathematical functions generally results from laboratory experiments on few *a priori* expected representative species and may not be suitable for extrapolation to ocean simulations that need to represent the large range of organisms present in oceanic ecosystems (Schartau et al., 2017; Ward et al., 2010). Furthermore, the assimilation of physical data in coupled physical-BGC models that improves the physical ocean state can paradoxically degrade the simulation of the BGC state of the ocean (Fennel et al., 2019; Park et al., 2018; Gasparin et al., 2021). A rigorous validation of BGC models is thus essential to test their predictive skills, their ability to reproduce BGC processes and estimate confidence intervals on model predictions (Doney et al., 2009; Stow et al., 2009).¶
¶
However, the validation of BGC models is presently limited by the availability of data. It relies principally on comparison with surface quantities from satellite (such as chlorophyll-*a* concentrations), cruises observations, and few permanent oceanic stations (e.g., Doney et al., 2009; Dutkiewicz et al., 2015; Lazzari et al., 2012, 2016; Lynch et al., 2009; Séférian et al., 2013; Stow et al., 2009). All these datasets neither have a sufficient vertical or temporal resolution, nor a synoptic view, nor can provide all variables necessary to evaluate how models represent climate-relevant processes such as the air-sea CO_2 fluxes, the biological carbon pump, ocean acidification or deoxygenation.¶
¶
In 2016, the Biogeochemical-Argo (BGC-Argo) program was launched with the goal to operate a global array of 1000 BGC-Argo floats equipped with oxygen (O_2), chlorophyll *a* (Chl*a*) and nitrate (NO_3) concentrations, particulate backscattering (b_{bp}), pH and downwelling irradiance sensors (Biogeochemical-Argo Planning Group, 2016; Claustre et al., 2020). Although the planned number of 1000 floats has not been reached yet, the BGC-Argo program has already provided a large number of quality-controlled vertical profiles of O_2, Chl*a*, NO_3, b_{bp}, and pH (Fig. 1). With respect to O_2, Chl*a*, NO_3, and b_{bp}, the North Atlantic and the Southern Ocean are reasonably well sampled whereas pH is so far essentially sampled in the Southern Ocean. At regional scale, the Mediterranean Sea is also fairly well sampled by BGC-Argo floats (Salon et al., 2019; Terzić et al., 2019). However, there are still, large under-sampled areas, like the subtropical gyres or the sub-polar North Pacific. Neverthel ... [1]

seasonal forecasts as well as climate projections. However, these models are far from being flawless, mostly because there are still huge knowledge gaps in the understanding of key BGC processes and, as a result, the mathematical functions that describe BGC fluxes, and ecosystems dynamics are too simplistic (Schartau et al., 2017). For instance, most models do not include a radiative component for the penetration of solar radiation in the ocean. It has been nevertheless shown that coupling such a component with a BGC model improves the representation of the dynamics of phytoplankton in the lower euphotic zone (Dutkiewicz et al., 2015). Additionally, the parameterisation of the mathematical functions generally results from laboratory experiments on a few representative species and may not be suitable for extrapolation to ocean simulations that need to represent the large range of organisms present in oceanic ecosystems (Schartau et al., 2017; Ward et al., 2010). Furthermore, the assimilation of physical data in coupled physical-BGC models that improves the physical ocean state can paradoxically degrade the simulation of the BGC state of the ocean (Fennel et al., 2019; Park et al., 2018; Gasparin et al., 2021). A rigorous assessment of BGC models is thus essential to test their predictive skills and ability to reproduce BGC processes and estimate confidence intervals on model predictions (Doney et al., 2009; Stow et al., 2009).

However, the evaluation of BGC models is limited by the availability of data. It relies principally on a combination of different data sets from satellite (such as chlorophyll-*a* concentrations), cruises observations, permanent oceanic stations from large databases such as the WOD. (e.g., Doney et al., 2009; Dutkiewicz et al., 2015; Lazzari et al., 2012, 2016; Lynch et al., 2009; Séférian et al., 2013; Stow et al., 2009). All these datasets have neither a sufficient vertical or temporal resolution, nor a synoptic view, nor provide all variables necessary to evaluate how models represent climate-relevant processes such as the air-sea CO_2 fluxes, the biological carbon pump, ocean acidification or deoxygenation.

In 2016, the Biogeochemical-Argo (BGC-Argo) program was launched with the goal to operate a global array of 1000 BGC-Argo floats equipped with oxygen (O_2), chlorophyll *a* (Chl*a*) and nitrate (NO_3) concentrations, particulate backscattering (b_{bp}), pH and downwelling irradiance sensors (Biogeochemical-Argo Planning Group, 2016; Claustre et al., 2020). Although the planned number of 1000 floats has not been reached yet, the BGC-Argo program has already provided a large number of quality-controlled vertical profiles of O_2, Chl*a*, NO_3, b_{bp}, and pH (Fig. 1). With respect to O_2, Chl*a*, NO_3, and b_{bp}, the North Atlantic and the Southern Ocean are reasonably well sampled whereas pH is well sampled only in the

Southern Ocean. At the regional scale, the Mediterranean Sea is also fairly well sampled by BGC-Argo floats (Salon et al., 2019; Terzić et al., 2019). However, there are still large under-sampled areas like the Arctic ocean, subtropical gyres and the sub-polar North Pacific. Thanks to machine learning based methods (Bittig et al., 2018; Sauzède et al., 2017), floats equipped with O_2 sensors can be additionally used to derive vertical profiles of NO_3, phosphate (PO_4), silicate (Si), alkalinity (Alk), dissolved inorganic carbon (DIC), pH and pCO_2.

The BGC-Argo data set represents a significant improvement for the assessment of models comparing to large databases such as the World Ocean Database (WOD) (Boyer et al., 2013) or the Copernicus Marine Service in situ dataset (European Union-Copernicus Marine Service, 2015). Large databases are composed of data collected from various instrument types with heterogenous data sampling methodologies. Therefore, for a given variable, the accuracy numbers are not the same and change depending on the instrument type (European Union-Copernicus Marine Service, 2019). Consequently, this affects the overall accuracy over time due to the changing proportion of instrument types over the years. On the other hand, the BGC-Argo data set is an homogenous data set with strict and uniform sampling methodologies and data Quality-Control (QC) procedures. As a result, the BGC-Argo data set have a satisfactory level of accuracy, which remains stable over time (Johnson et al., 2017; Mignot et al., 2019). Moreover, the number of quality-controlled observations collected every year by the BGC-Argo fleet is now greater than any other data set (Claustre et al., 2020). Using the BGC-Argo dataset as the single evaluation data set is therefore a way to ensure consistent accuracy.

The BGC-Argo floats provide multivariate observations at high vertical and temporal resolutions and for long periods of time providing nearly continuous time series of the vertical distribution of several biogeochemical variables. This is not possible with discrete, univariate vertical samplings provided by cruise cast *in situ* measurements or from climatological values derived from the WOA. All these specificities overcome the limitations of the previous datasets, especially with respect to their univariate nature, as well as their limited vertical and temporal resolution. This opens new perspectives for the evaluation of BGC models(Gutknecht et al., 2019; Salon et al., 2019; Terzić et al., 2019).

The development of BGC models as well as the continuous increase in spatial and vertical resolutions has reached the point where the volume of model outputs has dramatically increase. Simplification techniques are therefore required to provide decipherable information on model predictive skill. Allen et al. (2007) proposed a methodology for reducing the spatial dimensions in model assessment exercises, thereby providing concise information about the model performance. They use an unsupervised learning algorithm to classify the Southern North Sea into 5 coherent BGC regions based on modelled time series of temperature, NO_3, NO_3, and Si concentrations. They then evaluated the predictive capabilities of the model in each BGC region (instead of at each grid point), thus greatly reducing the number of points to be validated. An additional method for reducing the dimensions of model-data comparison is the use of assessment metrics (Hipsey et al., 2020; Russell et al., 2018). In particular, metrics such as depth-averaged state variables (e.g., mixed layer averaged Chl*a*, NO_3, O_2, etc…), mass fluxes and process rates validation (e.g., primary production or division rates), or emergent properties validation [e.g., Deep Chlorophyll Maximum (DCM), or Oxygen Minimum Zone [OMZ]) are particularly useful to reduce the number of model's vertical layers to be compared with the observations.

The objectives of the present study are twofold. Our first aim is to propose a methodology that uses the BGC-Argo data set, an unsupervised learning algorithm and assessment metrics to simplify marine BGC model-data comparisons, and thus inform, in a concise way, about model performance. The second objective is to use this methodology to also identify ocean regions where the model-observations misfit is larger than the variability of the BGC-Argo data and thus inform the BGC-Argo observing system of regions that should be better sampled. The first step of the method consists in defining 23 assessment metrics that are used both to construct the BGC regions and then to compare the model outputs with the BGC-Argo data. Second, following the approach of Allen et al. (Allen et al., 2007), we use an unsupervised learning algorithm, here a K-means clustering technique, to classify the global ocean into 8 coherent BGC regions based on the climatological modelled time series of the 23 assessments metrics. In the last step, the skill of the model in predicting the assessment metrics is evaluated in each BGC-region, using the model efficiency statistical score. Unlike other statistical metrics such the correlation coefficient, the bias or the root mean square difference, that does not quantifies objectively whether the model performance is acceptable or not; the model efficiency calculates whether the model outperforms an observational climatology (Fennel et al., 2022). Finally, the method is implemented using the Copernicus

Marine Service global BGC forecasting system (European Union-Copernicus Marine Service, 2019).

The paper is organised as follows: section 2 presents the data sets used in the study. In section 3, we define the assessment metrics and we detail the K-means algorithm as well as the model efficiency statistical score. In section 4, we presents and discuss the results. Finally, section 5 concludes the study.

2. Data

a. BGC-Argo floats observations

The float data were downloaded from the Argo Coriolis Global Data Assembly Centre in France (ftp://ftp.ifremer.fr/argo). The CTD and trajectory data were quality controlled using the standard Argo protocol (Wong et al., 2015). The raw BGC signals were transformed to biogeochemical variables (i.e., O_2, Chl*a*, NO_3, b_{bp}, and pH) and quality-controlled according to international BGC-Argo protocols (Johnson et al., 2018b, a; Schmechtig et al., 2015, 2018; Thierry et al., 2018; Thierry and Bittig, 2018).

In the Argo data-system, the data are available in three data modes: “Real-Time”, ”Adjusted” and ”Delayed” (Bittig et al., 2019). In the “Real-time” mode, the raw data are converted into state variables and an automatic quality-control is applied to “flag” gross outliers. In the “Adjusted” mode, the “Real-time” data receive a calibration adjustment in an automated manner. In the “Delayed” mode, the “Adjusted” data are adjusted and validated by a scientific expert. While the “Real-Time” and “Adjusted” data are considered acceptable for operational application (data assimilation), the “Delayed” mode” is designed for scientific exploitation and represent the highest quality of data with the ultimate goal, when time-series with sufficient duration will have been acquired, to possibly extract climate-related trends (Bojinski et al., 2014). However, for some variables, only a limited fraction of data is accessible in “Delayed-Mode”. Consequently, for each variable, we selected the highest level of data modes, where at least 80 % of the data are available (see Table 1). Note that this criterion does not apply to O_2, where only delayed mode data were selected in order to generate the pseudo-observations from CANYON-B neural network (see after). We removed

Deleted: follow

Deleted: necessary to compare

Deleted: to floats’ observations

Deleted: show examples of diagnostic plots for displaying the metrics. In

Deleted: , we discuss metrics relative to optical properties in the water column. Finally, section 6 summarizes and

Deleted:
Data

BGC-Argo floats observations

The float data were downloaded from the Argo Coriolis Global Data Assembly Centre in France (ftp://ftp.ifremer.fr/argo). The CTD and trajectory data were quality controlled using the standard Argo protocol (Wong et al., 2015). The raw BGC signals were transformed to biogeochemical variables (i.e., O_2, Chl*a*, NO_3, b_{bp}, and pH) and quality-controlled according to international BGC-Argo protocols (Johnson et al., 2018b, a; Schmechtig et al., 2015, 2018; Thierry et al., 2018; Thierry and Bittig, 2018).

In the Argo data-system, the data are available in three data modes: “Real-Time”, ”Adjusted” and ”Delayed” (Bittig et al., 2019).

Deleted: variable

Deleted: .

data with missing location or time information and flagged as “Bad data” (flag =4). Depending on the parameter and the associated data mode, we also excluded data flagged as “potentially bad data” (flag=3) (see Table 1).

Particulate Organic Carbon (POC) concentrations were derived from b_{bp} observations. First, three consecutive low-pass filters were applied on the vertical profiles of b_{bp} to remove spikes (Briggs et al., 2011): a 2-point running median followed by a 5-point running minimum and 5-point running maximum. Then, the filtered b_{bp} profiles were converted into POC (mgC m^{-3}) using a simplified version of the empirical POC/b_{bp} algorithm developed by Gali et al. (2022), i.e , for depths larger than the mixed layer depth (MLD):

$$\frac{POC}{b_{bp}} = c + a \cdot e^{-0.001 \cdot b \cdot (z - MLD)}, \qquad (1)$$

$$z > MLD,$$

where c is a constant deep value and, b, the slope of the exponential decrease, sets to 12010 mgC m^{-3} m and 6.57,respectively, as proposed by Gali et al. (2022). The global coefficient a, is set to 37990 mgC m^{-3} m to be consistent with a relationship, developed for global surface applications (i.e, POC= 38687.27* $b_{bp}^{0.95}$) (European Union-Copernicus Marine Service, 2020). This relationship is based on a global database of *in situ* POC and satellite b_{bp} (Evers-King et al., 2017). In the mixed layer (ML), z is fixed at MLD, and the Eq. (1) simplifies to

$$\frac{POC}{b_{bp}} = c + a, \qquad (2)$$

$$z \leq MLD.$$

Finally, we complemented the existing BGC-Argo dataset with pseudo-observations of NO_3, PO_4 , Si, Alk, and DIC concentrations as well as pH and pCO_2 using the CANYON-B neural network (Bittig et al., 2018). CANYON-B estimates vertical profiles of nutrients as well as the carbonate system variables from concomitant measurements of float pressure, temperature, salinity, and O_2 qualified in “Delayed“ mode together with the associated geolocalization and date of sampling. CANYON-B was trained and validated using the GLODAPv2 data set (Key et al., 2015). The CANYON-B estimates of NO_3 and pH were merged with measured values on the rationale that CANYON-B estimates have RMS errors (

Deleted: First, three consecutive low-pass filters were applied on the vertical profiles of b_{bp} to remove spikes (Briggs et al., 2011): a 2-points running median followed by a 5-points running minimum and 5-points running maximum. Then, the filtered b_{bp} profiles were converted into POC using a POC vs bbp relationship developed for the global ocean (https://catalogue.marine.copernicus.eu/documents/QUID/CMEMS-MOB-QUID-015-010.pdf) based on a global database of *in situ* POC and satellite bbp (Evers-King et al., 2017). This relationship, POC= 38687.27* $b_{bp}^{0.95}$, developed for global applications, has been shown to outperform regional relationships, applied at global scales. Negative values resulting from this transformation were set to 0.

Formatted: Indent: First line: 0 cm, Don't adjust space between Latin and Asian text, Don't adjust space between Asian text and numbers

Deleted: (Bittig et al., 2018).

Deleted: floats

NO_3 = 0.7 µmol kg^{-1} , pH = 0.013) (Bittig et al., 2018) that are of the same order of magnitude as those of the BGC-Argo observations errors (NO_3 = 0.5 µmol kg^{-1}, pH = 0.07) (Mignot et al., 2019; Johnson et al., 2017) .

Finally, we verified that the RMS errors of BGC-Argo data (both measured and from CANYON-B estimates) are lower than the RMS difference between the model and BGC-Argo data, so that the comparison of simulated properties with the BGC-Argo data leads to a meaningful evaluation of the model performance. We believe it is reasonable to draw conclusions on the model uncertainty from BGC-Argo data as long as the BGC-Argo errors are much lower than the model-observations RMS difference.

b. Copernicus Marine Service global BGC Model

The global model simulation used in this study (see Appendix A.1) originates from the Global Ocean hydrodynamic-biogeochemical model implemented and operated by the Global Monitoring and Forecasting Center of the EU, the Copernicus Marine Service. It is based on the coupled NEMO–PISCES model and is constrained by the assimilation of satellite Chl*a* concentrations. The BGC model is forced offline by daily fields of ocean, sea ice and atmosphere. The ocean and sea ice forcing come from Mercator Ocean global high-resolution ocean model (Lellouche et al., 2018) that assimilates along-track altimeter data, satellite Sea Surface Temperature and Sea-Ice Concentration, and *in situ* temperature and salinity vertical profiles. The BGC model has a 1/4° horizontal resolution, 50 vertical levels (with 22 levels in the upper 100 m, the vertical resolution is 1 m near the surface and decreases to 450 m resolution near the bottom). It produces daily outputs of Chl*a*, NO_3, PO_4, Si, O_2, pH, DIC and Alk, and weekly outputs of POC (resampled offline from weekly to daily frequency through constant interpolation) from 2009 to 2020. Note that the method of linear resampling, while artificially increasing the number of data, could potentially bias the statistical results, especially in regions with poor data coverage. Then, following the approach of Gali et al. (2022), the POC simulated by the model corresponds to the sum of the two sizes classes of phytoplankton, the small detrital particles and microzooplankton modelled by PISCES. This particular combination of phytoplanktonic and non-phytoplanktonic organisms has been shown to match the small POC observed by the floats (Galí et al., 2021). The partial pressures

Deleted: (Bittig et al., 2018)
Formatted: English (UK)
Deleted: (Mignot et al., 2019; Johnson et al., 2017)
Formatted: English (UK)
Deleted: CMEMS
Deleted: ,
Deleted: Environment Monitoring
Deleted: (CMEMS).
Deleted: it
Deleted: (Lellouche et al., 2018)
Deleted: linear
Deleted: 2017
Deleted: Following
Deleted: (2021)
Deleted: (Galí et al., 2021)
Deleted: Partial

of CO_2 values are extrapolated in the mixed layer from the surface value estimated by the model. The Black Sea was not considered in the present analysis because the model solutions are of poor qualities. Finally, the daily model outputs were collocated in time and spacethe closest to the BGC-Argo floats positions, and they were interpolated to the sampling depth of the float observations. The characteristics of the model are further detailed in the appendix.

3. Methods

a. Assessment metrics

In this section, we present 23 metrics used for the clustering of the ocean and for the assessment of the model simulation with BGC-Argo data. The metrics are associated with the carbonate chemistry, the biological carbon pump, and oxygen levels. Most of the metrics evaluate the model state accuracy through the comparison of simulated state variables with BGC-Argo observations depth-averaged in the mixed (herenafter indicated with the subscript $_{mixed}$) and mesopelagic (herenafter indicated with the subscript $_{meso}$) layers. This two-layer comparison between model and BGC-Argo data provides an indirect evaluation of the key mesopelagic processes and fluxes associated with the carbonate chemistry, biological carbon pump and oxygen levels in the mixed, and mesopelagic layers. In addition, some of the metrics assess the skill of the model in capturing emergent properties, such as the nitracline, the DCM and the OMZs. The metrics are described below and summarized in Table 2. The definition of the metrics is the same for the model and the BGC-Argo data. The MLD is computed, following De Boyer et al. (2004), as the depth at which the change in potential density from its value at 10 m exceeded 0.03 kg m^{-3}. The mesopelagic layer is defined as the layer between the MLD and 1000m. For simplicity, we use a simplified definition of the mesopelagic layer proposed by Dall' Olmo and Mork (2014). In their study, this layer is comprised between the deepest of the euphotic layer depth and the MLD, and 1000 m. Given the importance of the MLD in the calculation of the metrics, we verified that the MLD is correctly represented in the model -- the overall mean square difference between the model and the data is equal to ~30% of the overall variance of the observations.

i. Carbonate chemistry

Deleted: calculated offline from the modelled DIC, Alk, temperature and salinity data using the seacarb program for R (https://CRAN.R-project.org/package=seacarb).

Deleted: very

Deleted: the

Deleted: <#>Metrics

Deleted: 22

Deleted: a

Deleted: air-sea CO_2 flux

Deleted: oceanic pH,

Deleted: and Oxygen minimum zones (OMZs).

Deleted:

Air-sea CO_2 flux

Deleted: air-sea CO_2 flux

Deleted: generally calculated

Deleted: a bulk formulation (Wanninkhof, 2014), $F_{CO2} = k\alpha(pCO_{2atm} - spCO_2)$, where F_{CO2} is the air-sea CO_2 flux, α is the CO_2 solubility in seawater, k is a gas transfer coefficient that depends on wind speed, $spCO_2$ is the partial pressure of CO_2 at the ocean's surface, and pCO_{2atm} is the partial pressure of CO_2 in the atmosphere. Among the uncertainties affecting the different components of the model CO_2 flux, BGC-Argo data can contribute to estimate that on $spCO_2$. Thus, the validation of pCO_2 plays a critical role to assess the skill of a BGC model in representing correctly the air-sea CO_2 flux.

Here, $spCO_2$ is defined as the average of pCO_2 profile between the surface and the mixed layer depth (MLD). Following

Deleted: the MLD is computed

Deleted: We

Deleted: global bias

Deleted: BGC-Argo

Deleted: is 0.3 m.

Formatted: Font: 16 pt, Bold

Formatted: Indent: First line: 0 cm

Deleted: <#>Oceanic pH

Ocean acidification is the decrease in oceanic pH due to the absorption of anthropogenic CO_2. The acidification of the ocean is expected to impact primarily the surface oceanic waters as well as the 200-400 m layer (Kwiatkowski et al., 2020). Assessing how models correctly represent oceanic pH at the surface and in the 200-400 m layer is therefore critical if we aim to derive accurate climate projections on acidification. The surface ocean pH (spH) is defined as the average of pH profile between the surface and the base of the mixed layer and the pH in the 200-400 m layer ($pH_{200-400}$) as the average of pH profile in this layer.

Biological carbon pump

The biological carbon pump is the transformation of nutrients and dissolved inorganic carbon into organic carbon in the upper part of the ocean through phytoplankton photosynthesis and the subsequent transfer of this organic material into the deep ocean. The functioning of this pump relies on key pools of nutrients and carbon as well as several processes that control mass fluxes between the pools.

The first level of assessment of a biological carbon pump simulated by a model consists in evaluating the different ... [2]

The uptake of ~26 % anthropogenic CO_2 by the global ocean (Friedlingstein et al., 2022) has altered the oceanic carbonate chemistry over the past few decades (Iida et al., 2020). Assessing how models correctly represent the oceanic carbonate chemistry is therefore critical if we aim to derive accurate climate projections on their future change. The classical variables for the study of carbonate chemistry are DIC, Alk, pH and pCO_2 (Williams and Follows, 2011). These variables are assessed in the mixed (DIC_{mixed}, Alk_{mixed}, pH_{mixed} and $pCO_{2\ mixed}$) and mesopelagic (DIC_{meso}, Alk_{meso}, pH_{meso}) layers. The partial pressure of CO_2 is only assessed in the mixed layer as the evaluation of $pCO_{2\ mixed}$ plays a critical role to assess the skill of a BGC model to correctly represent the air-sea CO_2 flux.

ii. Biological carbon pump

The biological carbon pump is the transformation of nutrients and dissolved inorganic carbon into organic carbon in the upper part of the ocean through phytoplankton photosynthesis and the subsequent transfer of this organic material into the deep ocean. The functioning of this pump relies on key pools of nutrients and carbon as well as several processes that control mass fluxes between the pools. Changes in the biological carbon pump are now manifesting globally (Capuzzo et al., 2018; Osman et al., 2019; Roxy et al., 2016).

An indirect evaluation of the model capability to capture key processes associated with the biological carbon pump in the ocean upper layer, such as primary production, respiration, and grazing consists in comparing the different ML pools [here the nutrients ($NO_{3\ mixed}$, $PO_{4\ mixed}$, Si_{mixed}), Chl_{mixed} and POC_{mixed}] with BGC-Argo observations. Similarly, the assessment of the mesopelagic nutrients, and POC concentration (hereinafter denoted $NO_{3\ meso}$, $PO_{4\ meso}$, Si_{meso}, and POC_{meso}) provides an indirect evaluation of the key mesopelagic layer processes, such as export production, respiration, etc.

In stratified systems, a DCM is formed at the base of the euphotic layer (Barbieux et al., 2019; Cullen, 2015; Letelier et al., 2004; Mignot et al., 2014, 2011). It has been suggested that the DCM plays a key role in the synthesis of organic carbon by phytoplankton (Macías et al., 2014). DCMs are therefore key features to be assessed in BGC models with respect to processes involved in the biological carbon pump such as the primary production. However the DCM layer generally escapes detection by remote sensing. Furthermore, the DCM is also

Deleted: of

Deleted: . A second level assessment would be to directly compare these key processes with measured mass fluxes, but this assessment level is not addressed in this study. The surface nutrients, DIC, Chla and POC (hereinafter denoted sNO3, sPO4, sSi, sDIC, sChl and sPOC) are calculated as the average concentrations in the mixed layer.

Deleted: DIC

Deleted: indicated with the subscript

Deleted:)

Formatted: Font: 7 pt

Deleted: The mesopelagic concentrations are calculated as the depth-averaged concentrations between the base of the mixed layer down to 1000 m.

Deleted: In stratified systems, a Chl*a* maximum (hereinafter denoted Deep Chlorophyll Maximum, DCM) is formed at the base of the euphotic layer (Barbieux et al., 2019; Cullen, 2015; Letelier et al., 2004; Mignot et al., 2014, 2011). It has been suggested that the DCM plays an important role in the synthesis of organic carbon by phytoplankton (Macías et al., 2014). DCMs are therefore important features to be assessed in BGC models with respect to processes involved in the biological carbon pump processes such as the primary production, however the DCM layer generally escapes detection by remote sensing. Furthermore, DCM is also an emergent feature that develops in response to complex physical and biogeochemical interactions (Cullen, 2015). Thus, its evaluation provides critical information regarding the accuracy of the model in capturing complex patterns of key ecosystem processes. The depth and magnitude of DCM (H_{dcm} and Chl_{dcm}) are helpful metrics for the assessment of DCM dynamics. The depth of the DCM is calculated as the depth where the maximum of Chl*a* occurs in the profile with the criterion that H_{dcm} should be deeper than the MLD. The magnitude of the DCM is computed at the value at H_{dcm}.

The vertical supply of NO3 to the surface layers is a critical process of the biological carbon pump as NO3 is often depleted in the surface layers and is a limiting factor for phytoplankton growth in most oceanic regions. This NO3 vertical supply depends, among other factors, on the vertical gradient of NO3 (the nitracline), and, in particular, on its depth (the nitracline depth) (Cermeno et al., 2008; Omand and Mahadevan, 2015). Therefore, the comparison of the simulated nitracline depth with BGC-Argo observations allows for an indirect assessment of the model quality in reproducing vertical fluxes of NO3. Following previous studies (Cermeno et al., 2008; Lavigne et al., 2013; Richardson and Bendtsen, 2019), the depth of the nitracline corresponds to the first depth where NO3 is detected. The detection threshold is set to 1 µmol kg^{-1}, which corresponds to an upper estimate of BGC-Argo NO3 data accuracy (Johnson et al., 2017; Mignot et al., 2019).

an emergent feature that develops in response to complex physical and biogeochemical interactions (Cullen, 2015). Thus, its evaluation provides critical information regarding the accuracy of the model in capturing complex patterns of key ecosystem processes. The depth and magnitude of DCM (H_{DCM} and Chl_{DCM}) are helpful metrics for the assessment of DCM dynamics. The depth of the DCM is calculated as the depth where the maximum of Chl*a* occurs in the profile with the criterion that H_{DCM} should be deeper than the MLD. The magnitude of the DCM is computed at the value at H_{DCM}.

NO_3 is often depleted in the surface layers and is a limiting factor for phytoplankton growth in most oceanic regions. The vertical supply of NO_3 to the surface layers depends, among other factors, on the vertical gradient of NO_3 (the nitracline), and, in particular, on its depth (the nitracline depth) (Cermeno et al., 2008; Omand and Mahadevan, 2015). Therefore, the comparison of the simulated nitracline depth (H_{nit}) with BGC-Argo observations allows for an indirect assessment of the model performance in reproducing vertical fluxes of NO_3. Following previous studies (Cermeno et al., 2008; Lavigne et al., 2013; Richardson and Bendtsen, 2019), the depth of the nitracline corresponds to the first depth where NO_3 is detected. The detection threshold is set to 1 µmol kg^{-1}, which corresponds to an upper estimate of BGC-Argo NO_3 data accuracy (Johnson et al., 2017; Mignot et al., 2019).

iii. Oxygen levels

Oxygens levels in the global and coastal waters have declined over the whole water column over the past decades (Schmidtko et al., 2017) and OMZs are expanding (Stramma et al., 2008). Assessing how models correctly represent ocean oxygen levels as well as the OMZs is therefore critical to monitor their change over time. Similarly to DCMs, the assessment of OMZs is also informative on how the model simulates emergent dynamics as OMZs originate from complex physical and biogeochemical interactions (Paulmier and Ruiz-Pino, 2009). Oxygen levels are evaluated in the mixed ($O_{2\ mixed}$) and mesopelagic ($O_{2\ meso}$) layers. OMZs are defined as oceanic regions where O_2 levels are lower than 20 µmol kg^{-1} (Paulmier and Ruiz-Pino, 2009). OMZs are characterized by their depths (H_{O2min}) and their concentrations (O_{2min}).

b. Bioregionalization of the model

Deleted: and oxygen minimum zones

Formatted

Moved (insertion) [1]

Moved (insertion) [2]

In this study, we use the K-means clustering algorithm (Hartigan and Wong, 1979) to regionalize the ocean based on the modelled climatological monthly time series of the 23 metrics described previously. The K-means clustering is an unsupervised machine learning algorithm that combine similar objects into a group in such a way that, within a group, the similarity between objects is maximum and between groups, the similarity between objects is minimum. This clustering tool has been successfully used to classify marine BGC regions in different oceanic basins based on the seasonal cycle of satellite chlorophyll (Kheireddine et al., 2021; Mayot et al., 2016; Lacour et al., 2015; D'Ortenzio and d'Alcala, 2009) . The step-by-step methodology, used in this study, is described in the next section.

First, the climatological monthly time series of the 23 metrics were calculated at each model grid cell from the climatological monthly time series of the state variables predicted by the model from 2009 to 2017. The metrics in units of Chl*a* or POC were log-10 transformed to account for the fact that these metrics span several orders of magnitude and are lognormally distributed. Second, to take into consideration the 6-month shift in seasons between the northern and southern hemispheres, the dates for grid cells located in the Southern Hemisphere were shifted by 6 months (Bock et al., 2022). Third, to classify the model grid cells regardless of the different units of the 23 metrics, each metric was rescaled by subtracting the global mean and by dividing the global standard deviation. As a result, each metric had a mean of 0 and standard deviation of 1. Fourth, to reduce the dimensionality of the data set, a principal component analysis was applied to the scaled data. Only the components that explain 99 % of the variance in the data set were kept, reducing thereby the dimensions of the data set by 85 %. A K-means clustering analysis was then performed on the resulting data set. Following Kheireddine et al. (2021), the number of clusters was determined based on a silhouette analysis (Rousseeuw, 1987), and, as a result, was set to 8 .

c. Model efficiency

To quantify the model predictive skill, a model efficiency statistical score (m_e) was computed for each metric and in each BGC region:

$$m_e = 1 - \frac{\sum_{i=1}^{N}(m_i - o_i)^2}{\sum_{i=1}^{N}(o_i - \sigma)^2}, \qquad (3)$$

where m_i and o_i are the model and BGC-Argo matched values, respectively and σ is the BGC-Argo climatology. Assuming that the spatial variations are small in a given BGC-region, σ represents the temporal average and $\sum_{i=1}^{N}(o_i - \sigma)^2$ represents the variance due to temporal fluctuations. The model efficiency tests whether the model outperforms the BGC-Argo climatology ($0 < m_e < 1$,Fennel et al., 2022), or stated differently, if the model-data mean square difference is lower than the observation variance, i.e., $\sum_{i=1}^{N}(m_i - o_i)^2 < \sum_{i=1}^{N}(o_i - \sigma)^2$. To ensure the robustness of m_e, we verified that the number of matchups for each metric and in each BGC-region was greater than 100, then outliers were removed using Tukey's fences (Tukey, 1977).

Moved (insertion) [3]

Formatted: Font: 14 pt, Bold

Formatted: Indent: First line: 0 cm

4. Results and discussion

a. Global BGC-regions

The K-means clustering algorithm identified 8 distinct BGC-regions (Figure 2). 6 of the 8 BGC-regions correspond to well-defined spatial regions and are, thus, named accordingly, i.e., the Arctic, Equatorial, Mediterranean Sea, OMZs, Subtropical Gyres and Southern Oceans BGC-regions. The two others BGC-regions are located in the North Atlantic, North Pacific and North of the Southern Oceans BGC-region. These two BGC-regions correspond to ocean basins that are characterized by a phytoplankton "bloom" during spring time (Westberry et al., 2016), with the only difference that in one of the BGC-region, macronutrients such as nitrate and phosphate remains abundant throughout the year due to phytoplankton growth being mainly limited by iron (Williams and Follows, 2011). Accordingly, these two regions are named , Low Nutrients Bloom and High Nutrients Bloom, respectively. Finally, it should be noted that, outlier grid cells were no removed, and are mainly present in grid cells close to the coast. Furthermore, grid cells with bathymetry shallower than 1000 m, are not included in the clustering as metrics associated with the mesopelagic processes cannot be calculated in these shallow grid cells.

The BGC-regions found in study are overall coherent with the biomes estimated in Fay and McKinley (2014) (hereinafter denoted FM2014). The Arctic and Southern Oceans correspond to the FM2014 ice biome. The Subtropical Gyres correspond to the FM2014 subtropical permanently stratified biome . The Equatorial BGC-region represents a larger area than the Equatorial biome in FM2014. The Low Nutrients and High nutrients Bloom regions correspond to FM2014 subtropical seasonally stratified and subpolar seasonally stratified biomes, respectively. These two BGC-regions are coherent in the North Pacific and in the Southern Ocean in both studies. They differ, however, in the North Atlantic. In FM2014, the subpolar North Atlantic is divided between the subtropical seasonally stratified and subpolar seasonally stratified biomes, whereas in our study this area is only represented by one BGC-region; the Low Nutrients Bloom region. Finally, the Mediterranean sea and OMZs BGC-regions are not represented in FM2014. The main differences observed between our study and FM2014 stem from the fact our bioregionalization is based on 23 input variables while the clustering in FM14 is only based on one BGC input variable (Chla) and three physical variables (sea surface temperature, MLD and sea-ice faction). Therefore, our methodology can identified specific BGC-regions whose function is mainly characterized by variables other than Chl*a* (e.g. OMZs). Our method also include coastal areas, and identify the Mediterranean Sea which is not included in FM2014 because it is considered as a coastal region.

b. Model performance

Figures 3-5 show the m_e calculated for each assessment metric and in each BGC region. For clarity, the m_e are grouped by process (carbonate chemistry, biological carbon pump and oxygen levels). The results are presented as bubble plots (panels b) where the size of the bubble is proportional to the value of m_e. For a given assessment metric, the median value of m_e over all BGC regions are represented as a bar plot (panels c). Similarly, for a given BGC region, the median value of m_e over all assessment metrics is represented as a bar plot (panels a). When the number of assessment metrics is lower than 3, the mean value is computed instead of the median. In panels b, The x and y axes are arranged in descending order of the median value of m_e over all assessment metrics (panels a) and the median value of m_e over all BGC regions (panel b), respectively.

i. Carbonate chemistry

Overall, the model results in better predictions for Alk_{meso}, DIC_{mixed} , Alk_{mixed} , DIC_{meso} and pH_{meso} than the BGC-Argo climatology (m_e >1) (Figs. 3b and 3C) . The median m_e value for these metrics are (0.84, 0.78, 0.60, 0.57, and 0.56). For pH_{meso}, the model outperforms the BGC-Argo climatology in all BGC-regions. For Alk_{meso}, DIC_{mixed} , Alk_{mixed} , the model errors are lower than the variability of the observations everywhere except in the Arctic BGC-region. DIC_{meso} is better predicted by the model than the BGC-Argo climatology in almost all BGC-regions except in the Arctic, Southern Oceans, and the Mediterranean Sea . The model's ability to reproduce the instantaneous variability of pH_{mixed} and $pCO_{2\ mixed}$ is more limited. The model outperform the BGC-Argo climatology in only 4 BGC-regions for pH_{mixed} and 2 BGC-regions for $pCO_{2\ mixed}$. Overall, the carbonate chemistry dynamics is better estimated by the model than the BGC-Argo climatology in all BGC-regions except in the Arctic BGC-region (Fig. 3a)

ii. Biological carbon pump

The model efficiency is more limited for the biological carbon pump (Figs 4b and 4c). The model results in significant better estimations than the BGC-Argo climatology only for nutrients in the mesopelagic layer (Si_{meso}, $PO_{4\ meso}$ and $NO_{3\ meso}$), and H_{nit} (Fig. 4c). The model efficiency in predicting nutrients deteriorates when we move from the mesopelagic to the mixed layer, where the median m_e values drop from 0.83, 0.78, 0.68 to -2.10 and 0.1 , 0.08 for Si, PO_4 and NO_3 respectively. For the metrics associated with the first trophic level (i.e, Chl_{mixed}, H_{DCM}, Chl_{DCM}, POC_{mixed}, and POC_{meso}), the median m_e values are lower than 0 in almost all BGC-regions, suggesting than the model is almost systematically outperformed by the BGC-Argo climatology. Regionally, the median *me* values are greater than 1 only in the Low Nutrients and High Nutrients Bloom, the Mediterranean Sea and the OMZs BGC-regions.

Moved (insertion) [4]

iii. Oxygen levels

The model errors for $O_{2\ mixed}$ are lower than the data variability in all BGC-regions (Fig. 5b). In the mesopelagic layer, the model results also in better predictions than the BGC-Argo climatology everywhere except in the Southern Oceans and in the Arctic BGC-regions. The Oxygen Minimum Zones are detected in both the Equatorial and OMZs BGC regions. The magnitude of OMZs in both regions are better represented by the BGC-Argo climatology than the model, whereas the depth of the OMZ is better predicted by the model only in the OMZs region.

iv. Discussion

The skill of the model to surpass the BGC-Argo climatology for DIC, Alk and O_2 in the mesopelagic and the mixed layers is not surprising. As detailed in the appendix, the model applies a climatological damping,- to NO_3, PO_4, O_2, Si - with World Ocean Atlas 2013 (Garcia et al., 2013, 2014) - and to DIC and Alk– with GLODAPv2 climatology (Key et al., 2015). The damping mitigates the impact of the physical data assimilation in the offline coupled hydrodynamic-biogeochemical system, that results in an unrealistic drift of various biogeochemical variables (Fennel et al., 2019; Park et al., 2018; Gasparin et al., 2021).

Following this reasoning, one should also expect the nutrients to be better estimated by the model than by the BGC-Argo climatology. While, this is true in the mesopelagic layer, the model performance is significantly deteriorated in the mixed layer. In addition to the climatological damping, the model also embeds a reduced order Kalman filter (Lellouche et al., 2013) that assimilates daily L4 remotely sensed surface Chl*a* that provide a correction in the mixed layer to the modelled Chl*a* (both in the nanophytoplankton and diatom compartments) as well as to nitrate through the use of model error covariance. We verified that the assimilation of satellite Chl*a* decrease the model-BGC-argo data misfit comparing to a simulation without assimilation (not shown). We can, therefore speculate that uncertain model error covariance during the assimilation of satellite Chl*a* degrades the model skill in predicting ML nutrients. This hypothesis could be tested by computing the model efficiencies for a model simulation with only the climatological damping activated.

While the assimilation decreases the model-BGC-argo data misfit for Chl_{mixed} comparing to a simulation without assimilation (not shown), the model errors for the three metrics associated with Chl*a* remains systematically larger than the BGC-Argo variability. Yet, it has been shown that, when comparing to the satellite Chl*a* product assimilated (European Union-

Copernicus Marine Service, 2022), the model-satellite misfit was lower than the variability of the satellite data (European Union-Copernicus Marine Service, 2019). This suggest that the model-BGC-Argo data misfit could originate, in part, from discrepancies between the satellite Chl*a* product assimilated and the BGC-Argo data. We propose that studies should check the consistency between ocean colour products and BGC-Argo Chl*a* products at the global scale as these two products are expected to be assimilated together in future operational BGC systems (Ford, 2021).

Overall, the model also performs worse than the BGC-Argo climatology in predicting POC concentrations, the OMZs, pH_{mixed} and $pCO_{2\ mixed}$. The poor performance of PISCES-based models relative to BGC-Argo POC observations has been extensively studied in Gali et al. (2022). They pointed out that the large model-data misfit could be the result of an imperfect BGC-Argo POC-b_{bp} conversion factor, unsuitable model parameters associated with POC dynamics and missing processes in the model structure. Similarly, the poor model skill in capturing the OMZs dynamics are also already been documented in several studies (Busecke et al., 2022; Schmidt et al., 2021; Cabré et al., 2015). All studies suggested that improving the ocean circulation in physical models may be the most important factor to improve the accuracy of OMZs model predictions. Finally, the negative model efficiencies for pH_{mixed} and $pCO_{2\ mixed}$ could be understood by considering that pH and pCO_2 are driven by DIC, Alk, temperature and salinity. Consequently, the model uncertainties in pH_{mixed} and $pCO_{2\ mixed}$ are also controlled by the model errors in these 4 variables. Therefore, even small errors in modelled DIC, Alk (Fig. 3b) as well as modelled temperature and salinity (Lellouche et al., 2018) could lead to a poor model performance in capturing the variability of pH and pCO_2.

c. Recommendation for the design of the BGC-Argo observing system

Observing System Simulation Experiments (OSSE) have been the primary tool to inform about the design of the BGC-Argo observing system (Ford, 2021; Biogeochemical-Argo Planning Group, 2016). OSSEs typically comprises a realistic “nature run”, which represents “the truth” from which synthetic observations are sampled. The synthetic observations represents the observing system to be designed. To test its impact on improving models predictive skill, the synthetic observations are then assimilated in an “assimilative run”. The accuracy of the “assimilative run” is then evaluated against the “nature run”. Here, we use the real BGC-Argo observations to inform about the design of the BGC-Argo network. More specifically, our aim is to inform about the regions where the model errors are greater than the variability of the BGC-Argo data, and consequently where BGC-Argo observations should be enhanced to improve the model accuracy through BGC-Argo data assimilation or process-oriented assessment studies.

For a given BGC-region, we compute a single multivariate score which correspond to the median of the 23 m_e associated with each assessment metric (Fig. 6). This is consistent with the fact that the BGC-Argo floats, that are now deployed, observe the 5 variables used to derive the assessments metrics, i.e., O_2, Chl*a*, NO_3, b_{bp} and pH. The Arctic BGC-region is the only region whose median m_e is negative (-0.75). This is consistent with the fact that only 4 assessment metrics (namely $NO_{3\ meso}$, POC_{meso}, pH_{meso}, pH_{mixed}) are better represented by the model than the BGC-Argo climatology in this region (Figs. 3 and 4). Few BGC-Argo observations exist in this region (Fig.1), and, the winter-spring months are particularly under-sampled (not shown). In this region, satellite observations of Chl*a* are not possible most of year and the scarcity of in situ observations probably make the climatological damping less efficient in this region. Given the rapid changes occurring in the Arctic biogeochemical processes and ecosystems due to climate change (Solan et al., 2020), we strongly recommend to enhance the Arctic region with BGC-Argo floats. These observations are critical to better constrain the model. Given also the key role of the Southern Oceans and the Equatorial regions for the oceanic CO_2 cycle (Long et al., 2021; Landschützer et al., 2014), we also recommend to enhance these two regions whose median m_e are barely greater than 0 (0.04 and 0.12, respectively).

5. Conclusion

In this study, we propose a method based on the global data set of BGC-Argo observations, a K-means clustering algorithm and 23 assessments metrics to simplify model-data comparison and inform on Copernicus Marine Service forecasting system predictive skill and the design of the BGC-Argo observing system. The K-means algorithm identified 8 BGC-regions in the model simulation that are consistent with Fay and McKinley (2014) study. Within each

Moved up [1]: Oxygens levels in the global and coastal waters have declined over the whole water column over the past decades

Moved up [2]: . Assessing how models correctly represent ocean oxygen levels as well as the OMZs is therefore critical to monitor their change over time.

Moved up [3]: Results

Moved up [4]: 4c).

Deleted: (Schmidtko et al., 2017) and OMZs are expanding (Stramma et al., 2008)

Deleted: Similarly to DCMs, the assessment of OMZs is also informative on how the model simulates emergent dynamics as OMZs originate from complex physical and biogeochemical interactions (Paulmier and Ruiz-Pino, 2009). We evaluate oxygen levels in 3 layers, at the surface, at 300 m and at 1000 m. The surface O_2 (sO_2), important for the air-sea O_2 flux, is defined as the average of O_2 profile in the mixed layer. The oxygen at 300 m ($O_{2\ 300}$), a depth where large areas of the global ocean have very low O_2 (Breitburg et al., 2018), is defined as the average of O_2 profile between 250 and 300 m. The deep oxygen content, ($O_{2\ 1000}$), is defined as the average of O_2 profile between 950 and 1000 m. Finally, to characterize the OMZs, we evaluate the depth (H_{O2min}) and concentration (O_{2min}) of O_2 minimums. O_2 level lower than 80 µmol kg^{-1} are used to characterize OMZs (Schmidtko et al., 2017).

Diagnostic plots to display the BGC-Argo based metrics

Based upon the existing literature (e.g., Aumont et al., 2015; Cossarini et al., 2019; Doney et al., 2009; Dutkiewicz et al., 2015; Gutknecht et al., 2019; Salon et al., 2019; Séférian et al., 2013; Terzić et al., 2019), we propose 4 graphical representations that can be used to display the novel validation metrics and to assess the skill of a model in reproducing a particular process or variable: Taylor diagrams, scatterplots, spatial maps, and time series.

Taylor diagram

Taylor diagrams are useful to display simultaneously information on model-data skill for a suite of metrics (Taylor, 2001). These diagrams combine the Pearson correlation coefficient (r), root-mean-square difference (RMSD) and the model standard deviation (SD). In order to represent all metrics with different units into a single diagram, we use a normalized Taylor diagram (RMSD and the model SD are divided by the SD of the observations). In the diagram, the Pearson correlation coefficient between the model and the observations is related to the azimuthal angle. The normalized SDs are proportional to the radial distances from the origin. The observational reference is indicated along the x-axis and corresponds to the normalized S ... [3]

Deleted: **: Application to CMEMS global model**

Examples of the diagnostic plots described in section 4 in combination with the metrics defined in Section 3 are shown. The objective of this section is to illustrate the opportunities offered by the BGC-Argo data for evaluating global BGC model solutions, rather than to provide a full evaluation of the CMEMS global ... [4]

Deleted: The RMS difference between the predicted and the observed values seems to be quite uniform, suggesting the uncertainty in model sChl is fairly constant in all oceanic basins.

Seasonal time-series ... [5]

Formatted: Font: 14 pt, Bold

Deleted: Biogeochemical ocean models are powerful tools to monitor changes in marine ecosystems and ecosystem health due to human activities, make climate projections and help developing better strategies for mitigation. However, these models are subject to flaws and require rigorous validation processes to test their predictive skills. The model’s evaluations have long been damped by the ... [6]

BGC-region and for each assessment metric, we compute a model efficiency statistical score that quantify whether the model outperforms the BGC-Argo climatology by comparing the model-BGC-Argo data mean square difference with the observation variance.

Overall, the model surpasses the BGC-Argo climatology in predicting pH, DIC, Alk and O_2 in the mesopelagic and the mixed layers, as well as NO_3, Si and PO_4 in the mesopelagic layer. Concerning the other metrics, whose model predictions are outperformed by the BGC-Argo climatology, we provide suggestions to reduce the model-data misfit and thus to increase the model efficiency. For, PO_4, Si, and NO_3, we propose to test if the uncertain model error covariances during the assimilation of satellite Chl*a* could lead to a degradation in predicting nutrients in the mixed layer. For Chl*a*-related metrics, we recommend to check the consistency between ocean colour products and BGC-Argo Chl*a* products at the global scale as it may explain part of the misfit between the model, that assimilates satellite Chl*a*, and BGC-Argo observations. The discrepancies between modelled and observed POC and OMZs have been already investigated in previous studies. It has been suggested that improving the BGC-Argo POC-b_{bp} conversion factor, tuning the model parameters and implementing missing processes in the model structure could decrease the model-data inconsistencies associated with POC dynamics. Similarly, the improvement of the ocean circulation in physical models should improve the accuracy of OMZs model predictions. Finally, pH_{mixed} and $pCO_{2\ mixed}$ should be better modelled if the uncertainties associated with DIC, Alk, temperature and salinity in the mixed layer are reduced.

The method proposed here is also beneficial to inform about the BGC-Argo network design. In particular, the regions where BGC-Argo observations should be enhanced to reduce the model-data misfit through the assimilation of BGC-Argo data or process-oriented assessment studies. We strongly recommend to enhance the Arctic region, which is critically under sampled and is constantly outperformed by the BGC-Argo climatology. Likewise, BGC-Argo observations should be enriched in the Equatorial region and in the Southern Oceans, two regions where the model error barely exceed the BGC-Argo observations variability.

Tables

Table 1. Data mode and QC flags of the BGC-Argo observations used in this study. In the Argo data-system, the data are available in three data modes, “Real-Time”, ”Adjusted” and ”Delayed”. See section 2a for a brief description of each data mode. The flags “3” and “4” refers to “potentially bad data “ and “bad data”, respectively. See also Bittig et al. (2019), for a more detailed description of Argo data modes and flags.

Deleted: (2019)

Parameter	Data mode	Data mode of associated pressure, temperature and salinity profiles	QC flags
Chl*a*	Adjusted and Delayed	Real time, Adjusted and Delayed	• Real time: All flags except 4 • Adjusted or Delayed: All flags except 3 and 4
O_2	Delayed	Delayed	• All flags except 3 and 4
NO_3	Adjusted and Delayed	Real time, Adjusted and Delayed	• Real time: All flags except 4 • Adjusted or Delayed: All flags except 3 and 4
pH	Adjusted and Delayed	Real time, Adjusted and Delayed	• Real time: All flags except 4 • Adjusted or Delayed: All flags except 3 and 4
b_{bp}	Real time and Delayed	Real time, Adjusted and Delayed	• Real time: All flags except 4 • Adjusted or Delayed (P,T,S): All flags except 3 and 4

1

- Adjusted or Delayed (b_{bp}): All flags 4

Table 2. Assessment metrics used to assess the model simulation with BGC-Argo data . For each metric, the level of assessment, as described in Hipsey et al. (2020) is also indicated.

Process	Metric	Definition	units	Assessment level
Carbonate chemistry	$pCO_{2\ mixed}$	Depth-averaged pCO_2 in the mixed layer	μatm	State variable
	DIC_{mixed}	Depth-averaged DIC in the mixed layer	μmol kg^{-1}	State variable
	Alk_{mixed}	Depth-averaged Alk in the mixed layer	μmol kg^{-1}	State variable
	DIC_{meso}	Depth-averaged DIC in the mesopelagic layer	μmol kg^{-1}	State variable
	Alk_{meso}	Depth-averaged Alk in the mesopelagic layer	μmol kg^{-1}	State variable
	pH_{mixed}	Depth-averaged pH in the mixed layer	total	State variable
	pH_{meso}	Depth-averaged pH in the mesopelagic layer	total	State variable
Biological carbon pump	Chl_{mixed}	Depth-averaged Chl*a* in the mixed layer	mg m^{-3}	State variable
	$NO_{3\ mixed}$	Depth-averaged NO_3 in the mixed layer	μmol kg^{-1}	State variable
	$PO_{4\ mixed}$	Depth-averaged PO_4 in the mixed layer	μmol kg^{-1}	State variable
	Si_{mixed}	Depth-averaged Si in the mixed layer	μmol kg^{-1}	State variable

Deleted: (2020)

Deleted: Air-sea $CO_{2\ flux}$

Deleted: $spCO_2$

Formatted Table

Moved (insertion) [5]

Moved (insertion) [6]

Moved (insertion) [7]

Deleted: Oceanic pH

Deleted: spH

Formatted: Subscript

Formatted Table

Deleted: $pH_{200\text{-}400}$

Deleted: 200-400 m

Deleted: sChl

Deleted: sNO_3

Deleted: sPO_4

Deleted: sSi

Moved up [5]: Depth-averaged DIC in the mixed layer

Moved up [7]: μmol kg^{-1}

Moved up [6]: State variable

Deleted: ¶
sDIC ... [7]

	$NO_{3\,meso}$	Depth-averaged NO_3 in the mesopelagic layer	µmol kg^{-1}	State variable
	$PO_{4\,meso}$	Depth-averaged PO_4 in the mesopelagic layer	µmol kg^{-1}	State variable
	Si_{meso}	Depth-averaged Si in the mesopelagic layer	µmol kg^{-1}	State variable
	POC_{mixed}	Depth-averaged POC in the mixed layer	mg m^{-3}	State variable
	POC_{meso}	Depth-averaged POC in the mesopelagic layer	mg m^{-3}	State variable
	Chl_{DCM}	Magnitude of DCM	mg m^{-3}	Emergent property
	H_{DCM}	Depth of DCM	m	Emergent property
	H_{nit}	Depth of nitracline	m	Emergent property
Oxygen levels	$O_{2\,mixed}$	Depth-averaged O_2 in the mixed layer	µmol kg^{-1}	State variable
	$O_{2\,meso}$	Depth-averaged O_2 in the mesopelagic layer	µmol kg^{-1}	State variable
	O_{2min}	value of O_2 minimum	µmol kg^{-1}	Emergent property
	H_{O2min}	Depth of O_2 minimum	m	Emergent property

Deleted: ¶ DIC_{meso} ... [8]

Deleted: sPOC

Deleted: and OMZs

Deleted: sO_2

Deleted: lixed

Deleted: 300

Deleted: O_2 at 300 m

Deleted: ¶ $O_{2\,1000}$ ... [9]

Figures

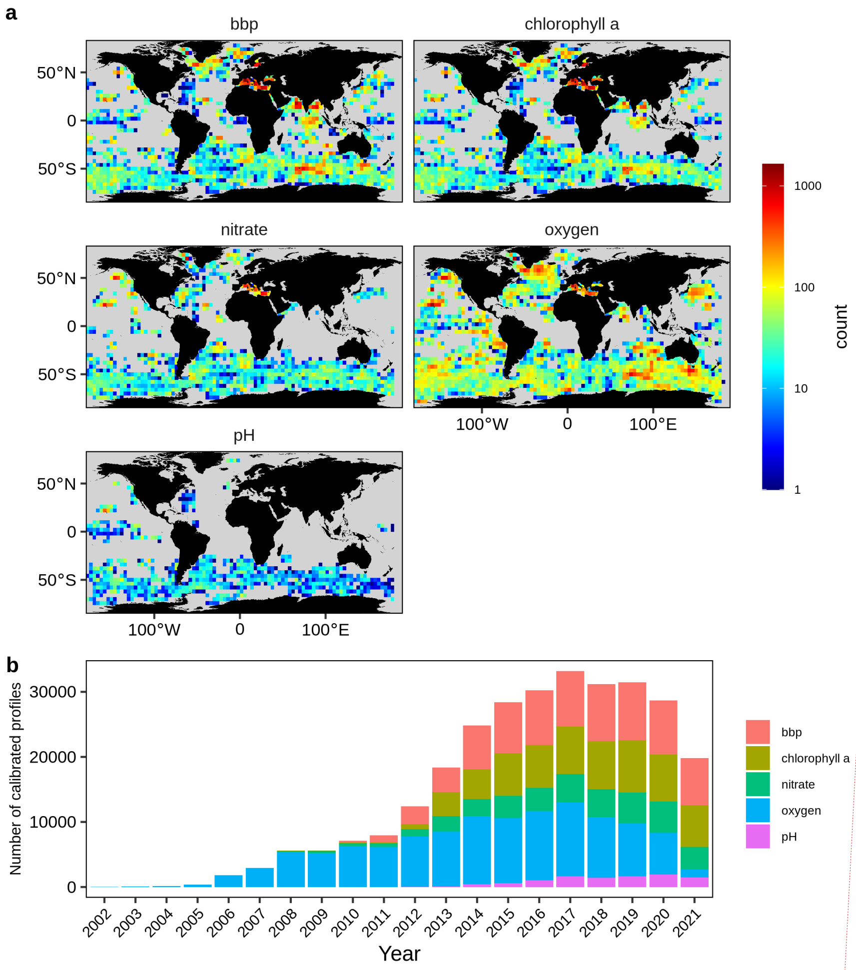

Figure 1. Spatial and temporal coverage of quality-controlled BGC-Argo pH, NO_3^-, Chl*a,* O_2, and b_{bp} profiles. **(a)** Number of quality-controlled profiles for the entire period per 4°x4° bin. **(b)** Number of quality-controlled profiles per year.

Deleted: ¶
Table 3. Global model skill assessment. The assessment metrics are defined in Table 2. ¶
Metric ... [10]

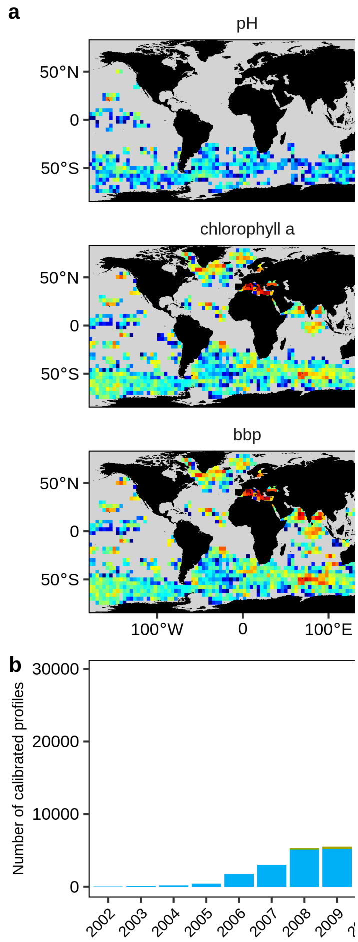

Deleted:

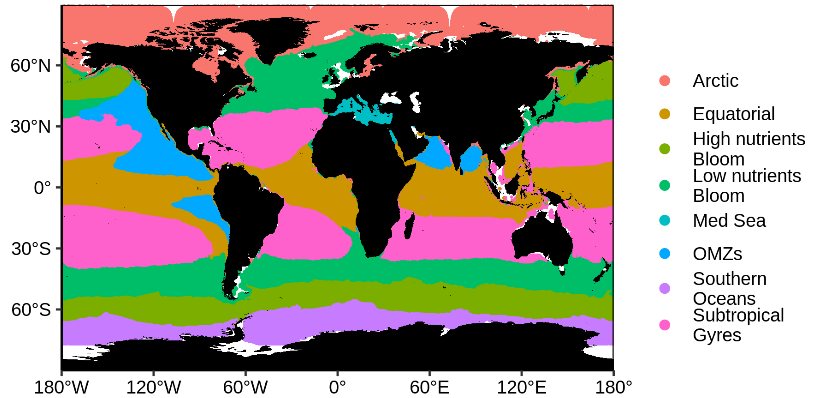

Figure 2. Spatial distribution of the 8 BGC-regions obtained with a K-means clustering method applied to a dataset of modelled climatological monthly time series of the 23 assessment metrics.

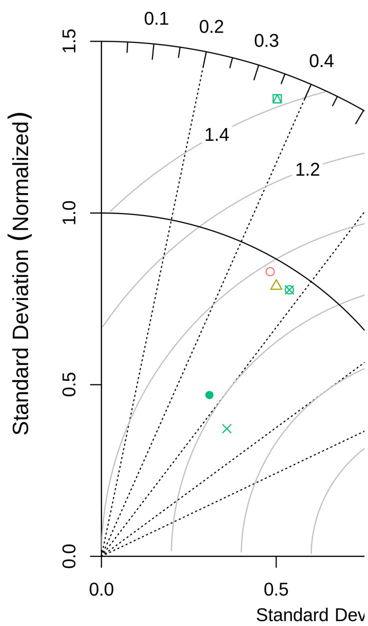

Deleted:
Figure 2. Comparison of BGC-Argo floats' observations and model values for all metrics using Taylor diagram. The symbols correspond to the metrics and the colours represent the BGC processes with which they are associated. Note that the metrics calculated from the float pH and NO_3 used both the direct observations of the floats and as well as the estimations from CANYON-B. The metrics related to Chl*a* and POC, namely sChl, Chl_{DCM}, sPOC, POC_{meso} were log_{10}-transformed because they cover several orders of magnitude and they are lognormally distributed. Observed DCMs and nitracline deeper than 250 m are not included.

... [11]

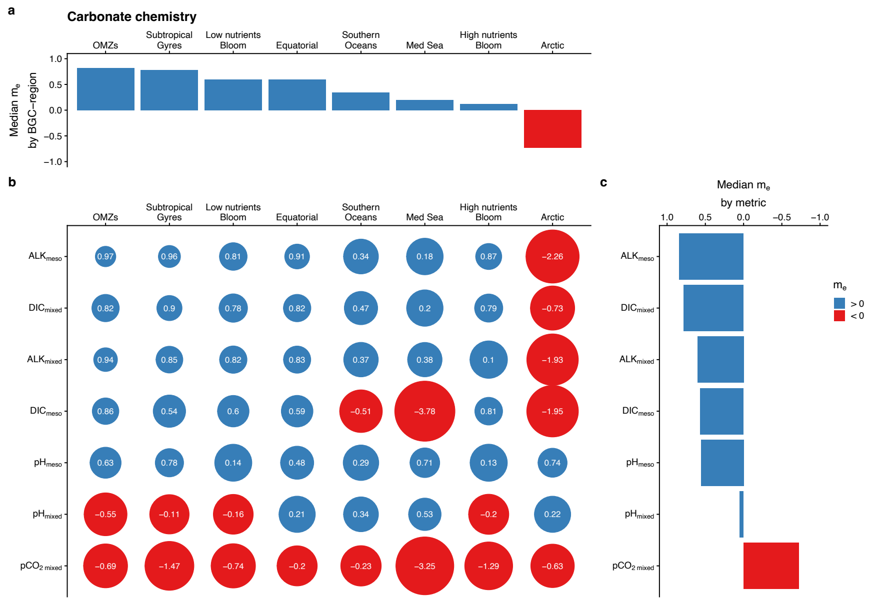

Figure 3. Bubble plot of model efficiency statistical score (m_e) as a function of BGC-regions and assessment metrics associated with the carbonate chemistry (**b**). The size of a bubble is proportional to the value of m_e. For a given assessment metric, the median value of m_e over all BGC regions are represented as a bar plot (**c**). Similarly, for a given BGC region, the median value of m_e over all assessment metrics is represented as a bar plot (**a**). In (**b**), The x and y axes are arranged in descending order of the median value of m_e over all assessment metrics (panels a) and the median value of m_e over all BGC regions, respectively. The blue and red colours correspond to a positive and negative m_e .

Figure 4. Same as Figure 3 but for assessment metrics associated with the biological carbon pump.

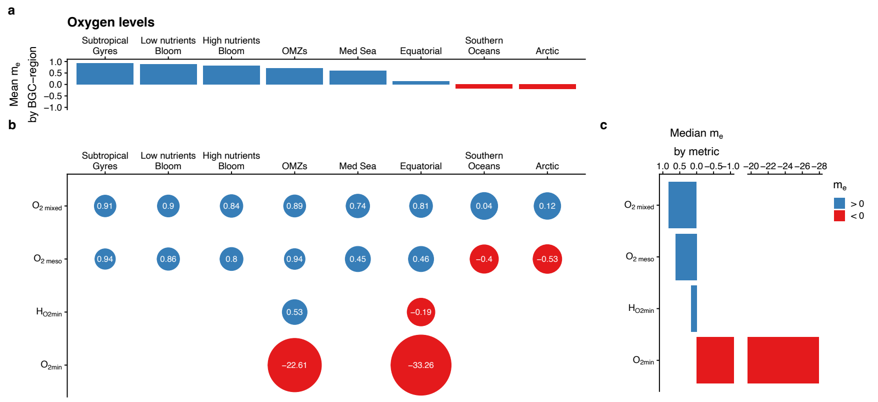

Figure 5. Same as Figure 3 but for assessment metrics associated with the oxygen levels. Note that in **(a)**, the bar plot represents the mean value of m_e over all assessment metrics.

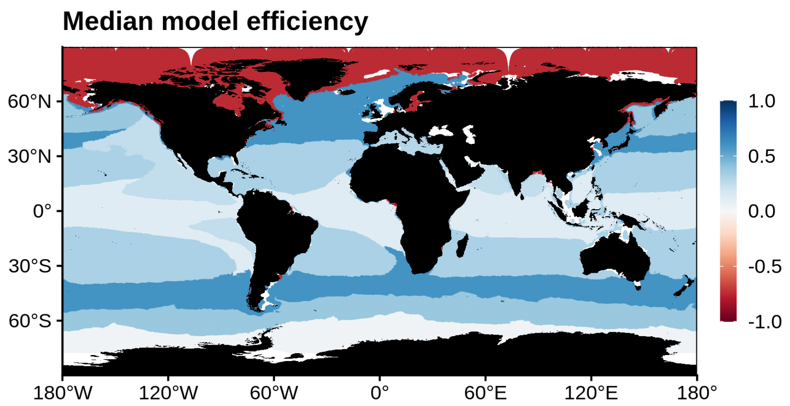

Figure 6. Median of the 23 m_e associated with each assessment metric by BGC-region.

Formatted: Font: Bold

Formatted: Line spacing: 1,5 lines

Appendix

A.1 The CMEMS global hydrodynamic-biogeochemical model

The model used in this study features the offline coupled NEMO–PISCES model, with a 1/4° horizontal resolution 50 vertical levels (with 22 levels in the upper 100 m, the vertical resolution is 1m near the surface and decreases to 450m resolution near the bottom) and daily temporal resolution, covering the period from 2009 to 2017.

The biogeochemical model PISCES v2 (Aumont et al., 2015) is a model of intermediate complexity designed for global ocean applications, and is part of NEMO modelling platform. It features 24 prognostic variables and includes five nutrients that limit phytoplankton growth (nitrate, ammonium, phosphate, silicate and iron) and four living compartments: two phytoplankton size classes (nanophytoplankton and diatoms, resp. small and large) and two zooplankton size classes (microzooplankton and mesozooplankton, resp. small and large); the bacterial pool is not explicitly modelled. PISCES distinguishes three non-living detrital pools for organic carbon, particles of calcium carbonate and biogenic silicate. Additionally, the model simulates the carbonate system and dissolved oxygen. PISCES has been successfully used in a variety of biogeochemical studies, both at regional and global scale (Bopp et al., 2005; Gehlen et al., 2006, 2007; Gutknecht et al., 2019; Lefèvre et al., 2019; Schneider et al., 2008; Séférian et al., 2013; Steinacher et al., 2010; Tagliabue et al., 2010).

The dynamical component is the latest Mercator Ocean global 1/12° high-resolution ocean model system, extensively described and validated in Lellouche et al. (2013, 2018). This system provides daily and 1/4°-coarsened fields of horizontal and vertical current velocities, vertical eddy diffusivity, mixed layer depth, sea ice fraction, potential temperature, salinity, sea surface height, surface wind speed, freshwater fluxes and net surface solar shortwave irradiance that drive the transport of biogeochemical tracers. This system also features a reduced-order Kalman filter based on the Singular Evolutive Extended Kalman filter (SEEK) formulation introduced by Pham et al. (1998), that assimilates, on a 7-day assimilation cycle, along-track altimeter data, satellite Sea Surface Temperature and Sea-Ice Concentration from

Deleted: (Aumont et al., 2015)

Field Code Changed

Deleted:
The dynamical component is the latest Mercator Ocean global 1/12° high-resolution ocean model system, extensively described and validated in Lellouche et al. (2013, 2018). This system provides daily and 1/4°-coarsened fields of horizontal and vertical current velocities, vertical eddy diffusivity, mixed layer depth, sea ice fraction, potential temperature, salinity, sea surface height, surface wind speed, freshwater fluxes and net surface solar shortwave irradiance that drive the transport of biogeochemical tracers. This system also features a reduced-order Kalman filter based on the Singular Evolutive Extended Kalman filter (SEEK) formulation introduced by Pham et al. (1998), that assimilates, on a 7-day assimilation cycle, along-track altimeter data, satellite Sea Surface Temperature and Sea-Ice Concentration from OSTIA, and *in situ* temperature and salinity vertical profiles from the CORA 4.2 in situ database.

OSTIA, and *in situ* temperature and salinity vertical profiles from the CORA 4.2 in situ database.

In addition, the biogeochemical component of the coupled system also embeds a reduced order Kalman filter (similar to the above mentioned) that operationally assimilates daily L4 remotely sensed surface chlorophyll (European Union-Copernicus Marine Service, 2022). Thanks to a multivariate formulation of model error covariances, the system is able to provide a 3D correction to the nanophytoplankton, diatoms and nitrates model concentrations, from the surface chlorophyll data provided by satellite observations.

In parallel, a climatological-damping is applied to nitrate, phosphate, oxygen, silicate - with World Ocean Atlas 2013 - to dissolved inorganic carbon and alkalinity – with GLODAPv2 climatology (Key et al., 2015) - and to dissolved organic carbon and iron - with a 4000-year PISCES climatological run. This relaxation is set to mitigate the impact of the physical data assimilation in the offline coupled hydrodynamic-biogeochemical system, leading significant rises of nutrients in the Equatorial Belt area, and resulting in an unrealistic drift of various biogeochemical variables e.g. chlorophyll, nitrate, phosphate (Fennel et al., 2019; Park et al., 2018). The time-scale associated with this climatological damping is set to 1 year and allows a smooth constraint that has been shown to be efficient to reduce the model drift.

Deleted: (https://resources.marine.copernicus.eu/documents/QUID/CMEMS-GLO-QUID-001-028.pdf).

Deleted: (Key et al., 2015)

Deleted: (Fennel et al., 2019; Park et al., 2018)

Deleted:

A.2 The Mediterranean Sea biogeochemical model MedBFM

The Mediterranean Sea biogeochemical model MedBFM, is based on the system described in Teruzzi et al. (2014) and Salon et al. (2019).

The physical forcing fields needed to compute the transport include the 3-d horizontal and vertical current velocities, vertical eddy diffusivity, potential temperature, and salinity and 2-d data surface data for wind stress. These forcing datasets are simulated by the Mediterranean Sea Monitoring and Forecasting Centre (MED–MFC) in the Copernicus Marine Environmental Monitoring Service (CMEMS, http://marine.copernicus.eu). The biogeochemical model is then offline forced adopting the output computed by the CMEMS MED-MFC. In the present application, we switched off the biogeochemical assimilation scheme that is currently used in the operational MED-MFC system.

The light propagation is resolved coupling an atmospheric multispectral radiative transfer model (Lazzari et al., 2020) with an in-water radiative model (Dutkiewicz et al., 2015) featuring bands at 25 nm resolution in the UV and visible wavelengths.

The horizontal resolution is approximately 6 km and there are 72 vertical levels with 3 m resolution at surface coarsening at 300 m for the deeper layers. The biogeochemical model here adopted (Biogeochemical Flux Model -- BFM -- ; (Vichi et al., 2015)) has been already applied to simulate primary producers biogeochemistry (Lazzari et al., 2012), alkalinity spatial and temporal variability (Cossarini et al., 2015), and CO_2 fluxes (Canu et al., 2015) for the Mediterranean Sea, and has been corroborated using *in situ* data for the operational purposes within CMEMS (Salon et al., 2019). The BFM model has been expanded in the present configuration adding the dynamics of coloured dissolved organic carbon (CDOM) by assuming a constant CDOM:DOC production ratio (i.e. 2%, as in (Dutkiewicz et al., 2015)). The absorption of CDOM, is described using reference absorption at 450 nm of 0.015 m2/mgC (Dutkiewicz et al., 2015) and an exponential slope of 0.017 nm^{-1} (Babin et al., 2003; Organelli et al., 2014).

A.3 BGC-Argo K_d estimates

The data used to compute the K_d metrics are quality checked according to Organelli et al. (2017). Moreover, for the K_d logarithmic interpolation, the following selection rules were applied: the profile must have at least 5 BGC Argo float sampling in the first optical depth, the gap between the two shallower acquisitions must be less than 10 meters, and there must be at least one measurement deeper than 15 meters.

A.4 Figures

... [12]

Data availability. The BGC model data can be downloaded from the Copernicus Marine Environmental Monitoring Service (https://resources.marine.copernicus.eu/?option=com_csw&view=details&product_id=GLOBAL_ANALYSIS_FORECAST_BIO_001_028). The BGC-Argo data were downloaded from the Argo Global Data Assembly Centre in France (ftp://ftp.ifremer.fr/argo/).

Deleted: https://resources.marine.copernicus.eu/?option=com_csw&view=details&product_id=GLOBAL_ANALYSIS_FORECAST_BIO_001_028).

Authors Contribution: AM, GC, FD, SS and VT originated the study. AM, HC, FD, RS and VT designated the study. AM and RS process the BGC-Argo floats data. AM analysed the data. AM wrote the first draft of the manuscript. HC, GC, FD, EG, PL, CP, SS,RS,VT and AT contributed to the subsequent drafts. All authors read and approved the final draft.

Deleted: PL processed the BGC-Argo float in the Mediterranean Sea and run the Mediterranean BGC model.

Competing Interests: The authors declare no competing financial interests.

Materials and correspondence: Correspondence and request for material should be addressed to mignot@mercator-ocean.fr

Acknowledgements: This study has been conducted using the Copernicus Marine Service products. The BGC-Argo data were collected and made freely available by the International Argo program and the national programs that contribute to it (https://www.argo.jcommops.org). The Argo program is part of the Global Ocean Observing System. Part of this work was performed within the framework of the BIOOPTIMOD and MASSIMILI CMEMS Service Evolution Projects. This paper represents a contribution to the following research projects: NAOS (funded by the Agence Nationale de la Recherche in the framework of the French "Equipement d'avenir" program, grant ANR J11R107-F), remOcean (funded by the European Research Council, grant 246777), and the French Bio-Argo program (BGC-Argo France; funded by CNES-TOSCA, LEFE-GMMC).

Deleted: (CMEMS).

References

Allen, J. I., Somerfield, P. J., and Gilbert, F. J.: Quantifying uncertainty in high-resolution coupled hydrodynamic-ecosystem models, J. Mar. Syst., 64, 3–14, https://doi.org/10.1016/j.jmarsys.2006.02.010, 2007.

Aumont, O., Ethé, C., Tagliabue, A., Bopp, L., and Gehlen, M.: PISCES-v2: an ocean biogeochemical model for carbon and ecosystem studies, Geosci. Model Dev., 8, 2465–2513, https://doi.org/10.5194/gmd-8-2465-2015, 2015.

Barbieux, M., Uitz, J., Gentili, B., Pasqueron de Fommervault, O., Mignot, A., Poteau, A., Schmechtig, C., Taillandier, V., Leymarie, E., Penkerc'h, C., D'Ortenzio, F., Claustre, H., and Bricaud, A.: Bio-optical characterization of subsurface chlorophyll maxima in the Mediterranean Sea from a Biogeochemical-Argo float database, Biogeosciences, 16, 1321–1342, https://doi.org/10.5194/bg-16-1321-2019, 2019.

Deleted: Babin, M., Stramski, D., Ferrari, G. M., Claustre, H., Bricaud, A., Obolensky, G., and Hoepffner, N.: Variations in the light absorption coefficients of phytoplankton, nonalgal particles, and dissolved organic matter in coastal waters around Europe, J. Geophys. Res. Oceans, 108, 2003.¶
Baird, M. E., Cherukuru, N., Jones, E., Margvelashvili, N., Mongin, M., Oubelkheir, K., Ralph, P. J., Rizwi, F., Robson, B. J., Schroeder, T., Skerratt, J., Steven, A. D. L., and Wild-Allen, K. A.: Remote-sensing reflectance and true colour produced by a coupled hydrodynamic, optical, sediment, biogeochemical model of the Great Barrier Reef, Australia: Comparison with satellite data, Environ. Model. Softw., 78, 79–96, https://doi.org/10.1016/j.envsoft.2015.11.025, 2016.¶

Biogeochemical-Argo Planning Group: The scientific rationale, design and implementation plan for a Biogeochemical-Argo float array, https://doi.org/10.13155/46601, 2016.

Bittig, H. C., Steinhoff, T., Claustre, H., Fiedler, B., Williams, N. L., Sauzède, R., Körtzinger, A., and Gattuso, J.-P.: An alternative to static climatologies: robust estimation of open ocean CO2 variables and nutrient concentrations from T, S, and O2 data using Bayesian neural networks, Front. Mar. Sci., 5, 328, 2018.

Bittig, H. C., Maurer, T. L., Plant, J. N., Wong, A. P., Schmechtig, C., Claustre, H., Trull, T. W., Udaya Bhaskar, T. V. S., Boss, E., and Dall'Olmo, G.: A BGC-Argo guide: Planning, deployment, data handling and usage, Front. Mar. Sci., 6, 502, 2019.

Bock, N., Cornec, M., Claustre, H., and Duhamel, S.: Biogeographical Classification of the Global Ocean From BGC-Argo Floats, Glob. Biogeochem. Cycles, 36, https://doi.org/10.1029/2021GB007233, 2022.

Bojinski, S., Verstraete, M., Peterson, T. C., Richter, C., Simmons, A., and Zemp, M.: The concept of essential climate variables in support of climate research, applications, and policy, Bull. Am. Meteorol. Soc., 95, 1431–1443, 2014.

Bopp, L., Aumont, O., Cadule, P., Alvain, S., and Gehlen, M.: Response of diatoms distribution to global warming and potential implications: A global model study, Geophys. Res. Lett., 32, https://doi.org/10.1029/2005GL023653, 2005.

Boyer, T. P., Antonov, J. I., Baranova, O. K., Garcia, H. E., Johnson, D. R., Mishonov, A. V., O'Brien, T. D., Seidov, D., Smolyar, I., and Zweng, M. M.: World ocean database 2013, 2013.

Deleted: Bosc, E., Bricaud, A., and Antoine, D.: Seasonal and interannual variability in algal biomass and primary production in the Mediterranean Sea, as derived from 4 years of SeaWiFS observations, Glob. Biogeochem. Cycles, 18, https://doi.org/10.1029/2003GB002034, 2004.¶

Breitburg, D., Levin, L. A., Oschlies, A., Grégoire, M., Chavez, F. P., Conley, D. J., Garçon, V., Gilbert, D., Gutiérrez, D., Isensee, K., Jacinto, G. S., Limburg, K. E., Montes, I., Naqvi, S. W. A., Pitcher, G. C., Rabalais, N. N., Roman, M. R., Rose, K. A., Seibel, B. A., Telszewski, M., Yasuhara, M., and Zhang, J.: Declining oxygen in the global ocean and coastal waters, Science, 359, https://doi.org/10.1126/science.aam7240, 2018.

Briggs, N., Perry, M. J., Cetinić, I., Lee, C., D'Asaro, E., Gray, A. M., and Rehm, E.: High-resolution observations of aggregate flux during a sub-polar North Atlantic spring bloom, Deep Sea Res. Part Oceanogr. Res. Pap., 58, 1031–1039, https://doi.org/10.1016/j.dsr.2011.07.007, 2011.

Busecke, J. J. M., Resplandy, L., Ditkovsky, S. J., and John, J. G.: Diverging Fates of the Pacific Ocean Oxygen Minimum Zone and Its Core in a Warming World, AGU Adv., 3, https://doi.org/10.1029/2021AV000470, 2022.

Cabré, A., Marinov, I., Bernardello, R., and Bianchi, D.: Oxygen minimum zones in the tropical Pacific across CMIP5 models: mean state differences and climate change trends, Biogeosciences, 12, 5429–5454, https://doi.org/10.5194/bg-12-5429-2015, 2015.

Capuzzo, E., Lynam, C. P., Barry, J., Stephens, D., Forster, R. M., Greenwood, N., McQuatters-Gollop, A., Silva, T., van Leeuwen, S. M., and Engelhard, G. H.: A decline in primary production in the North Sea over 25 years, associated with reductions in zooplankton abundance and fish stock recruitment, Glob. Change Biol., 24, e352–e364, https://doi.org/10.1111/gcb.13916, 2018.

Cermeno, P., Dutkiewicz, S., Harris, R. P., Follows, M., Schofield, O., and Falkowski, P. G.: The role of nutricline depth in regulating the ocean carbon cycle, Proc. Natl. Acad. Sci., 105, 20344–20349, https://doi.org/10.1073/pnas.0811302106, 2008.

Claustre, H., Johnson, K. S., and Takeshita, Y.: Observing the Global Ocean with Biogeochemical-Argo, Annu. Rev. Mar. Sci., 12, annurev-marine-010419-010956, https://doi.org/10.1146/annurev-marine-010419-010956, 2020.

Crowder, L. B., Hazen, E. L., Avissar, N., Bjorkland, R., Latanich, C., and Ogburn, M. B.: The Impacts of Fisheries on Marine Ecosystems and the Transition to Ecosystem-Based Management, Annu. Rev. Ecol. Evol. Syst., 39, 259–278, https://doi.org/10.1146/annurev.ecolsys.39.110707.173406, 2008.

Cullen, J. J.: Subsurface Chlorophyll Maximum Layers: Enduring Enigma or Mystery Solved?, Annu. Rev. Mar. Sci., 7, 207–239, https://doi.org/10.1146/annurev-marine-010213-135111, 2015.

Dall'Olmo, G. and Mork, K. A.: Carbon export by small particles in the Norwegian Sea, Geophys. Res. Lett., 41, 2921–2927, https://doi.org/10.1002/2014GL059244, 2014.

Doney, S. C., Lima, I., Moore, J. K., Lindsay, K., Behrenfeld, M. J., Westberry, T. K., Mahowald, N., Glover, D. M., and Takahashi, T.: Skill metrics for confronting global upper ocean ecosystem-biogeochemistry models against field and remote sensing data, J. Mar. Syst., 76, 95–112, https://doi.org/10.1016/j.jmarsys.2008.05.015, 2009.

D'Ortenzio, F, and d'Alcala, M. R.: On the trophic regimes of the Mediterranean Sea: a satellite analysis, Biogeosciences, 6, 139–148, 2009.

Dutkiewicz, S., Hickman, A. E., Jahn, O., Gregg, W. W., Mouw, C. B., and Follows, M. J.: Capturing optically important constituents and properties in a marine biogeochemical and ecosystem model, Biogeosciences, 12, 4447–4481, https://doi.org/10.5194/bg-12-4447-2015, 2015.

Deleted: Campbell

Deleted: W.: The lognormal distribution as a model for bio-optical variability in

Deleted: sea, J. Geophys. Res. Oceans, 100, 13237–13254

Deleted: 95JC00458, 1995

Deleted: Canu, D. M., Ghermandi, A., Nunes, P. A., Lazzari, P., Cossarini, G., and Solidoro, C.: Estimating the value of carbon sequestration ecosystem services in the Mediterranean Sea: An ecological economics approach, Glob. Environ. Change, 32, 87–95, 2015.¶

Deleted: Cossarini, G., Lazzari, P., and Solidoro, C.: Spatiotemporal variability of alkalinity in the Mediterranean Sea, Biogeosciences, 12, 1647–1658, https://doi.org/10.5194/bg-12-1647-2015, 2015.¶
Cossarini, G., Mariotti, L., Feudale, L., Mignot, A., Salon, S., Taillandier, V., Teruzzi, A., and D'Ortenzio, F.: Towards operational 3D-Var assimilation of chlorophyll Biogeochemical-Argo float data into a biogeochemical model of the Mediterranean Sea, Ocean Model., 133, 112–128, https://doi.org/10.1016/j.ocemod.2018.11.005, 2019.¶

Deleted: Dale, T., Rey, F., and Heimdal, B. R.: Seasonal development of phytoplankton at a high latitude oceanic site, Sarsia, 84, 419–435, 1999.¶

Deleted: ., Lavigne, H., Besson, F., Claustre, H., Coppola, L., Garcia, N., Laes-Huon, A., Le Reste, S., Malarde, D., Migon, C., Morin, P., Mortier, L., Poteau, A., Prieur, L., Raimbault, P., and Testor, P.: Observing mixed layer depth, nitrate and chlorophyll concentrations in the northwestern Mediterranean: A combined satellite and NO3 profiling floats experiment, Geophys. Res. Lett., 41, 2014GL061020, https://doi.org/10.1002/2014GL061020, 2014

Eriksen, M., Lebreton, L. C. M., Carson, H. S., Thiel, M., Moore, C. J., Borerro, J. C., Galgani, F., Ryan, P. G., and Reisser, J.: Plastic Pollution in the World's Oceans: More than 5 Trillion Plastic Pieces Weighing over 250,000 Tons Afloat at Sea, PLoS ONE, 9, e111913, https://doi.org/10.1371/journal.pone.0111913, 2014.

European Union-Copernicus Marine Service: Global Ocean- In-Situ Near-Real-Time Observations, https://doi.org/10.48670/MOI-00036, 2015.

European Union-Copernicus Marine Service: Global Ocean Biogeochemistry Analysis and Forecast, https://doi.org/10.48670/MOI-00015, 2019.

European Union-Copernicus Marine Service: Global Ocean 3D Chlorophyll-a concentration, Particulate Backscattering coefficient and Particulate Organic Carbon, https://doi.org/10.48670/MOI-00046, 2020.

European Union-Copernicus Marine Service: Global Ocean Colour (Copernicus-GlobColour), Bio-Geo-Chemical, L4 (monthly and interpolated) from Satellite Observations (Near Real Time), https://doi.org/10.48670/MOI-00279, 2022.

Evers-King, H., Martinez-Vicente, V., Brewin, R. J. W., Dall'Olmo, G., Hickman, A. E., Jackson, T., Kostadinov, T. S., Krasemann, H., Loisel, H., Röttgers, R., Roy, S., Stramski, D., Thomalla, S., Platt, T., and Sathyendranath, S.: Validation and Intercomparison of Ocean Color Algorithms for Estimating Particulate Organic Carbon in the Oceans, Front. Mar. Sci., 4, 251, https://doi.org/10.3389/fmars.2017.00251, 2017.

Fay, A. R. and McKinley, G. A.: Global open-ocean biomes: mean and temporal variability, Earth Syst. Sci. Data, 6, 273–284, https://doi.org/10.5194/essd-6-273-2014, 2014.

Fennel, K., Gehlen, M., Brasseur, P., Brown, C. W., Ciavatta, S., Cossarini, G., Crise, A., Edwards, C. A., Ford, D., Friedrichs, M. A. M., Gregoire, M., Jones, E., Kim, H.-C., Lamouroux, J., Murtugudde, R., Perruche, C., and the GODAE OceanView Marine Ecosystem Analysis and Prediction Task Team: Advancing Marine Biogeochemical and Ecosystem Reanalyses and Forecasts as Tools for Monitoring and Managing Ecosystem Health, Front. Mar. Sci., 6, 89, https://doi.org/10.3389/fmars.2019.00089, 2019.

Fennel, K., Mattern, J. P., Doney, S. C., Bopp, L., Moore, A. M., Wang, B., and Yu, L.: Ocean biogeochemical modelling, Nat. Rev. Methods Primer, 2, 1–21, https://doi.org/10.1038/s43586-022-00154-2, 2022.

Ford, D.: Assimilating synthetic Biogeochemical-Argo and ocean colour observations into a global ocean model to inform observing system design, Biogeosciences, 18, 509–534, https://doi.org/10.5194/bg-18-509-2021, 2021.

Friedlingstein, P., O'Sullivan, M., Jones, M. W., Andrew, R. M., Gregor, L., Hauck, J., Le Quéré, C., Luijkx, I. T., Olsen, A., Peters, G. P., Peters, W., Pongratz, J., Schwingshackl, C., Sitch, S., Canadell, J. G., Ciais, P., Jackson, R. B., Alin, S. R., Alkama, R., Arneth, A., Arora, V. K., Bates, N. R., Becker, M., Bellouin, N., Bittig, H. C., Bopp, L., Chevallier, F., Chini, L. P., Cronin, M., Evans, W., Falk, S., Feely, R. A., Gasser, T., Gehlen, M., Gkritzalis, T., Gloege, L., Grassi, G., Gruber, N., Gürses, Ö., Harris, I., Hefner, M., Houghton, R. A., Hurtt, G. C., Iida, Y., Ilyina, T., Jain, A. K., Jersild, A., Kadono, K., Kato, E., Kennedy, D., Klein Goldewijk, K., Knauer, J., Korsbakken, J. I., Landschützer, P., Lefèvre, N., Lindsay, K., Liu, J., Liu, Z., Marland, G., Mayot, N., McGrath, M. J., Metzl, N., Monacci, N. M., Munro, D. R., Nakaoka, S.-I., Niwa, Y., O'Brien, K., Ono, T., Palmer, P. I., Pan, N., Pierrot, D., Pocock, K., Poulter, B., Resplandy, L., Robertson, E., Rödenbeck, C., Rodriguez, C., Rosan, T. M., Schwinger, J., Séférian, R., Shutler, J. D., Skjelvan, I., Steinhoff, T., Sun, Q., Sutton, A. J., Sweeney, C., Takao, S., Tanhua, T., Tans, P. P., Tian, X., Tian, H., Tilbrook, B., Tsujino, H., Tubiello, F., van der Werf, G. R., Walker, A. P., Wanninkhof, R., Whitehead, C., Willstrand Wranne, A., et al.: Global Carbon Budget 2022, Earth Syst. Sci. Data, 14, 4811–4900, https://doi.org/10.5194/essd-14-4811-2022, 2022.

Galí, M., Falls, M., Claustre, H., Aumont, O., and Bernardello, R.: Bridging the gaps between particulate backscattering measurements and modeled particulate organic carbon in the ocean, Biogeochemistry: Open Ocean, https://doi.org/10.5194/bg-2021-201, 2021.

Galí, M., Falls, M., Claustre, H., Aumont, O., and Bernardello, R.: Bridging the gaps between particulate backscattering measurements and modeled particulate organic carbon in the ocean, Biogeosciences, 19, 1245–1275, https://doi.org/10.5194/bg-19-1245-2022, 2022.

Garcia, H. E., Locarnini, R. A., Boyer, T. P., Antonov, J. I., Baranova, O. K., Zweng, M. M., Reagan, J. R., Johnson, D. R., Mishonov, A. V., and Levitus, S.: World ocean atlas 2013. Volume 4, Dissolved inorganic nutrients (phosphate, nitrate, silicate), 2013.

Garcia, H. E., Boyer, T. P., Locarnini, R. A., Antonov, J. I., Mishonov, A. V., Baranova, O. K., Zweng, M. M., Reagan, J. R., Johnson, D. R., and Levitus, S.: World ocean atlas 2013. Volume 3, Dissolved oxygen, apparent oxygen utilization, and oxygen saturation, 2014.

Gasparin, F., Cravatte, S., Greiner, E., Perruche, C., Hamon, M., Van Gennip, S., and Lellouche, J.-M.: Excessive productivity and heat content in tropical Pacific analyses: Disentangling the effects of in situ and altimetry assimilation, Ocean Model., 160, 101768, https://doi.org/10.1016/j.ocemod.2021.101768, 2021.

Gehlen, M., Bopp, L., Emprin, N., Aumont, O., Heinze, C., and Ragueneau, O.: Reconciling surface ocean productivity, export fluxes and sediment composition in a global biogeochemical ocean model, Biogeosciences, 3, 521–537, https://doi.org/10.5194/bg-3-521-2006, 2006.

Gehlen, M., Gangstø, R., Schneider, B., Bopp, L., Aumont, O., and Ethe, C.: The fate of pelagic $CaCO_3$ production in a high CO_2 ocean: a model study, Biogeosciences, 4, 505–519, https://doi.org/10.5194/bg-4-505-2007, 2007.

Gutknecht, E., Reffray, G., Mignot, A., Dabrowski, T., and Sotillo, M. G.: Modelling the marine ecosystem of Iberia-Biscay-Ireland (IBI) European waters for CMEMS operational applications, Ocean Sci., 15, 1489–1516, https://doi.org/10.5194/os-15-1489-2019, 2019.

Hartigan, J. A. and Wong, M. A.: Algorithm AS 136: A K-Means Clustering Algorithm, Appl. Stat., 28, 100, https://doi.org/10.2307/2346830, 1979.

Hipsey, M. R., Gal, G., Arhonditsis, G. B., Carey, C. C., Elliott, J. A., Frassl, M. A., Janse, J. H., de Mora, L., and Robson, B. J.: A system of metrics for the assessment and improvement of aquatic ecosystem models, Environ. Model. Softw., 128, 104697, https://doi.org/10.1016/j.envsoft.2020.104697, 2020.

Deleted: McGuire, P. C., Melton,

Deleted: . R

Deleted: Nabel, J. E. M. S.,

Deleted: Neill, C., Omar, A. M

Deleted: Peregon, A.,

Deleted: Rehder, G.,

Deleted: Séférian, R.,

Deleted: Smith, N.,

Deleted: . N

Deleted: Wiltshire

Deleted: J., and Zaehle, S

Deleted: 2019

Deleted: 11, 1783–1838

Deleted: 11-1783-2019, 2019

Deleted: Gittings, J. A., Raitsos, D. E., Kheireddine, M., Racault, M.-F., Claustre, H., and Hoteit, I.: Evaluating tropical phytoplankton phenology metrics using contemporary tools, Sci. Rep., 9, 1–9, 2019.
Gregg, W. W. and Rousseaux, C. S.: Directional and spectral irradiance in ocean models: effects on simulated global phytoplankton, nutrients, and primary production, Front. Mar. Sci., 3, 240, 2016.

Iida, Y., Takatani, Y., Kojima, A., and Ishii, M.: Global trends of ocean CO 2 sink and ocean acidification: an observation-based reconstruction of surface ocean inorganic carbon variables, J. Oceanogr., 1–36, 2020.

Johnson, Plant, J. N., Coletti, L. J., Jannasch, H. W., Sakamoto, C. M., Riser, S. C., Swift, D. D., Williams, N. L., Boss, E., Haëntjens, N., Talley, L. D., and Sarmiento, J. L.: Biogeochemical sensor performance in the SOCCOM profiling float array: SOCCOM BIOGEOCHEMICAL SENSOR PERFORMANCE, J. Geophys. Res. Oceans, 122, 6416–6436, https://doi.org/10.1002/2017JC012838, 2017.

Johnson, Plant, J. N., and Maurer, T. L.: Processing BGC-Argo pH data at the DAC level, 2018a.

Johnson, Pasqueron De Fommervault, O., Serra, R., D'Ortenzio, F., Schmechtig, C., Claustre, H., and Poteau, A.: Processing Bio-Argo nitrate concentration at the DAC Level, 2018b.

Key, R. M., Olsen, A., van Heuven, S., Lauvset, S. K., Velo, A., Lin, X., Schirnick, C., Kozyr, A., Tanhua, T., and Hoppema, M.: Global Ocean Data Analysis Project, Version 2 (GLODAPv2), Carbon Dioxide Information Analysis Center, Oak Ridge Nat Lab, 2015.

Kheireddine, M., Mayot, N., Ouhssain, M., and Jones, B. H.: Regionalization of the Red Sea Based on Phytoplankton Phenology: A Satellite Analysis, J. Geophys. Res. Oceans, 126, https://doi.org/10.1029/2021JC017486, 2021.

Deleted: Kwiatkowski, L., Torres, O., Bopp, L., Aumont, O., Chamberlain, M., Christian, J. R., Dunne, J. P., Gehlen, M., Ilyina, T., John, J. G., Lenton, A., Li, H., Lovenduski, N. S., Orr, J. C., Palmieri, J., Santana-Falcón, Y., Schwinger, J., Séférian, R., Stock, C. A., Tagliabue, A., Takano, Y., Tjiputra, J., Toyama, K., Tsujino, H., Watanabe, M., Yamamoto, A., Yool, A., and Ziehn, T.: Twenty-first century ocean warming, acidification, deoxygenation, and upper-ocean nutrient and primary production decline from CMIP6 model projections, Biogeosciences, 17, 3439–3470, https://doi.org/10.5194/bg-17-3439-2020, 2020.

Lacour, L., Claustre, H., Prieur, L., and D'Ortenzio, F.: Phytoplankton biomass cycles in the North Atlantic subpolar gyre: A similar mechanism for two different blooms in the Labrador Sea: THE LABRADOR SEA BLOOMS, Geophys. Res. Lett., 42, 5403–5410, https://doi.org/10.1002/2015GL064540, 2015.

Landschützer, P., Gruber, N., Bakker, D. C. E., and Schuster, U.: Recent variability of the global ocean carbon sink, Glob. Biogeochem. Cycles, 28, 927–949, https://doi.org/10.1002/2014GB004853, 2014.

Lavigne, H., D'Ortenzio, F., Migon, C., Claustre, H., Testor, P., d'Alcalà, M. R., Lavezza, R., Houpert, L., and Prieur, L.: Enhancing the comprehension of mixed layer depth control on the Mediterranean phytoplankton phenology: Mediterranean Phytoplankton Phenology, J. Geophys. Res. Oceans, 118, 3416–3430, https://doi.org/10.1002/jgrc.20251, 2013.

Lazzari, Solidoro, C., Ibello, V., Salon, S., Teruzzi, A., Béranger, K., Colella, S., and Crise, A.: Seasonal and inter-annual variability of plankton chlorophyll and primary production in the Mediterranean Sea: a modelling approach, Biogeosciences, 9, 217–233, https://doi.org/10.5194/bg-9-217-2012, 2012.

Lazzari, Solidoro, C., Salon, S., and Bolzon, G.: Spatial variability of phosphate and nitrate in the Mediterranean Sea: A modeling approach, Deep Sea Res. Part Oceanogr. Res. Pap., 108, 39–52, https://doi.org/10.1016/j.dsr.2015.12.006, 2016.

Lefèvre, N., Veleda, D., Tyaquiçã, P., Perruche, C., Diverrès, D., and Ibánhez, J. S. P.: Basin-Scale Estimate of the Sea-Air CO $_2$ Flux During the 2010 Warm Event in the Tropical North Atlantic, J. Geophys. Res. Biogeosciences, 124, 973–986, https://doi.org/10.1029/2018JG004840, 2019.

Deleted: Lazzari, Salon, S., Terzić, E., Gregg, W. W., D'Ortenzio, F., Vellucci, V., Organelli, E., and Antoine, D.: Assessment of the spectral downward irradiance at the surface of theMediterranean Sea using the OASIM ocean-atmosphere radiative model, Surface/Numerical Models/Mediterranean Sea/Air-sea fluxes/Oceanic ecosystems, https://doi.org/10.5194/os-2020-108, 2020.

Lellouche, Greiner, E., Le Galloudec, O., Garric, G., Regnier, C., Drevillon, M., Benkiran, M., Testut, C.-E., Bourdalle-Badie, R., Gasparin, F., Hernandez, O., Levier, B., Drillet, Y., Remy, E., and Le Traon, P.-Y.: Recent updates to the Copernicus Marine Service global ocean monitoring and forecasting real-time 1⁄12° high-resolution system, Ocean Sci., 14, 1093–1126, https://doi.org/10.5194/os-14-1093-2018, 2018.

Lellouche, J.-M., Le Galloudec, O., Drévillon, M., Régnier, C., Greiner, E., Garric, G., Ferry, N., Desportes, C., Testut, C.-E., Bricaud, C., Bourdallé-Badie, R., Tranchant, B., Benkiran, M., Drillet, Y., Daudin, A., and De Nicola, C.: Evaluation of global monitoring and forecasting systems at Mercator Océan, Ocean Sci., 9, 57–81, https://doi.org/10.5194/os-9-57-2013, 2013.

Letelier, R. M., Karl, D. M., Abbott, M. R., and Bidigare, R. R.: Light driven seasonal patterns of chlorophyll and nitrate in the lower euphotic zone of the North Pacific Subtropical Gyre, Limnol. Oceanogr., 49, 508–519, 2004.

Long, M. C., Stephens, B. B., McKain, K., Sweeney, C., Keeling, R. F., Kort, E. A., Morgan, E. J., Bent, J. D., Chandra, N., Chevallier, F., Commane, R., Daube, B. C., Krummel, P. B., Loh, Z., Luijkx, I. T., Munro, D., Patra, P., Peters, W., Ramonet, M., Rödenbeck, C., Stavert, A., Tans, P., and Wofsy, S. C.: Strong Southern Ocean carbon uptake evident in airborne observations, Science, 374, 1275–1280, https://doi.org/10.1126/science.abi4355, 2021.

Lynch, D. R., McGillicuddy, D. J., and Werner, F. E.: Skill assessment for coupled biological/physical models of marine systems, J. Mar. Syst., 1, 1–3, 2009.

Macías, D., Stips, A., and Garcia-Gorriz, E.: The relevance of deep chlorophyll maximum in the open Mediterranean Sea evaluated through 3D hydrodynamic-biogeochemical coupled simulations, Ecol. Model., 281, 26–37, 2014.

Mayot, N., D'Ortenzio, F., Ribera d'Alcalà, M., Lavigne, H., and Claustre, H.: Interannual variability of the Mediterranean trophic regimes from ocean color satellites, Biogeosciences, 13, 1901–1917, https://doi.org/10.5194/bg-13-1901-2016, 2016.

Mignot, Claustre, H., Uitz, J., Poteau, A., D'Ortenzio, F., and Xing, X.: Understanding the seasonal dynamics of phytoplankton biomass and the deep chlorophyll maximum in oligotrophic environments: A Bio-Argo float investigation, Glob. Biogeochem. Cycles, 28, 856–876, https://doi.org/10.1002/2013GB004781, 2014.

Mignot, A., Claustre, H., D'Ortenzio, F., Xing, X., Poteau, A., and Ras, J.: From the shape of the vertical profile of in vivo fluorescence to Chlorophyll-a concentration, Biogeosciences, 8, 2391–2406, https://doi.org/10.5194/bg-8-2391-2011, 2011.

Mignot, A., D'Ortenzio, F., Taillandier, V., Cossarini, G., and Salon, S.: Quantifying Observational Errors in Biogeochemical-Argo Oxygen, Nitrate, and Chlorophyll *a* Concentrations, Geophys. Res. Lett., 46, 4330–4337, https://doi.org/10.1029/2018GL080541, 2019.

Omand, M. M. and Mahadevan, A.: The shape of the oceanic nitracline, Biogeosciences, 12, 3273–3287, https://doi.org/10.5194/bg-12-3273-2015, 2015.

Deleted: Mignot, Ferrari, R., and Claustre, H.: Floats with bio-optical sensors reveal what processes trigger the North Atlantic bloom, Nat. Commun., 9, https://doi.org/10.1038/s41467-017-02143-6, 2018.

Osman, M. B., Das, S. B., Trusel, L. D., Evans, M. J., Fischer, H., Grieman, M. M., Kipfstuhl, S., McConnell, J. R., and Saltzman, E. S.: Industrial-era decline in subarctic Atlantic productivity, Nature, 569, 551–555, https://doi.org/10.1038/s41586-019-1181-8, 2019.

Park, J.-Y., Stock, C. A., Yang, X., Dunne, J. P., Rosati, A., John, J., and Zhang, S.: Modeling Global Ocean Biogeochemistry With Physical Data Assimilation: A Pragmatic Solution to the Equatorial Instability, J. Adv. Model. Earth Syst., 10, 891–906, https://doi.org/10.1002/2017MS001223, 2018.

Paulmier, A. and Ruiz-Pino, D.: Oxygen minimum zones (OMZs) in the modern ocean, Prog. Oceanogr., 80, 113–128, 2009.

Richardson, K. and Bendtsen, J.: Vertical distribution of phytoplankton and primary production in relation to nutricline depth in the open ocean, Mar. Ecol. Prog. Ser., 620, 33–46, https://doi.org/10.3354/meps12960, 2019.

Rousseeuw, P. J.: Silhouettes: A graphical aid to the interpretation and validation of cluster analysis, J. Comput. Appl. Math., 20, 53–65, https://doi.org/10.1016/0377-0427(87)90125-7, 1987.

Roxy, M. K., Modi, A., Murtugudde, R., Valsala, V., Panickal, S., Prasanna Kumar, S., Ravichandran, M., Vichi, M., and Lévy, M.: A reduction in marine primary productivity driven by rapid warming over the tropical Indian Ocean, Geophys. Res. Lett., 43, 826–833, https://doi.org/10.1002/2015GL066979, 2016.

Russell, J. L., Kamenkovich, I., Bitz, C., Ferrari, R., Gille, S. T., Goodman, P. J., Hallberg, R., Johnson, K., Khazmutdinova, K., and Marinov, I.: Metrics for the evaluation of the Southern Ocean in coupled climate models and earth system models, J. Geophys. Res. Oceans, 123, 3120–3143, 2018.

Salon, S., Cossarini, G., Bolzon, G., Feudale, L., Lazzari, P., Teruzzi, A., Solidoro, C., and Crise, A.: Novel metrics based on Biogeochemical Argo data to improve the model uncertainty evaluation of the CMEMS Mediterranean marine ecosystem forecasts, Ocean Sci., 15, 997–1022, https://doi.org/10.5194/os-15-997-2019, 2019.

Sauzède, R., Bittig, H. C., Claustre, H., Pasqueron de Fommervault, O., Gattuso, J.-P., Legendre, L., and Johnson, K. S.: Estimates of Water-Column Nutrient Concentrations and Carbonate System Parameters in the Global Ocean: A Novel Approach Based on Neural Networks, Front. Mar. Sci., 4, https://doi.org/10.3389/fmars.2017.00128, 2017.

Schartau, M., Wallhead, P., Hemmings, J., Löptien, U., Kriest, I., Krishna, S., Ward, B. A., Slawig, T., and Oschlies, A.: Reviews and syntheses: parameter identification in marine planktonic ecosystem modelling, Biogeosciences, 14, 1647–1701, https://doi.org/10.5194/bg-14-1647-2017, 2017.

Schmechtig, C., Poteau, A., Claustre, H., D'Ortenzio, F., and Boss, E.: Processing bio-Argo chlorophyll-A concentration at the DAC level, Ifremer, https://doi.org/10.13155/39468, 2015.

Schmechtig, C., Claustre, H., Poteau, A., and D'Ortenzio, F.: Bio-Argo quality control manual for the Chlorophyll-A concentration, Ifremer, https://doi.org/10.13155/35385, 2018.

Deleted: Organelli, E., Bricaud, A., Antoine, D., and Matsuoka, A.: Seasonal dynamics of light absorption by chromophoric dissolved organic matter (CDOM) in the NW Mediterranean Sea (BOUSSOLE site), Deep Sea Res. Part Oceanogr. Res. Pap., 91, 72–85, 2014.¶
Organelli, E., Barbieux, M., Claustre, H., Schmechtig, C., Poteau, A., Bricaud, A., Boss, E. B., Briggs, N., Dall'Olmo, G., and d'Ortenzio, F.: Two databases derived from BGC-Argo float measurements for marine biogeochemical and bio-optical applications, Earth Syst. Sci. Data, 9, 861–880, 2017.¶

Deleted: Plant, J. N., Johnson, K. S., Sakamoto, C. M., Jannasch, H. W., Coletti, L. J., Riser, S. C., and Swift, D. D.: Net community production at Ocean Station Papa observed with nitrate and oxygen sensors on profiling floats, Glob. Biogeochem. Cycles, 30, 859–879, https://doi.org/10.1002/2015GB005349, 2016.¶

Deleted: Riley, G.: Factors Controlling Phytoplankton Populations on Georges Bank, J. Mar. Res., 6, 54–73, 1946.¶

Schmidt, H., Getzlaff, J., Löptien, U., and Oschlies, A.: Causes of uncertainties in the representation of the Arabian Sea oxygen minimum zone in CMIP5 models, Ocean Sci., 17, 1303–1320, https://doi.org/10.5194/os-17-1303-2021, 2021.

Schmidtko, S., Stramma, L., and Visbeck, M.: Decline in global oceanic oxygen content during the past five decades, Nature, 542, 335–339, https://doi.org/10.1038/nature21399, 2017.

Schneider, B., Bopp, L., Gehlen, M., Segschneider, J., Frölicher, T. L., Cadule, P., Friedlingstein, P., Doney, S. C., Behrenfeld, M. J., and Joos, F.: Climate-induced interannual variability of marine primary and export production in three global coupled climate carbon cycle models, Biogeosciences, 5, 597–614, https://doi.org/10.5194/bg-5-597-2008, 2008.

Séférian, R., Bopp, L., Gehlen, M., Orr, J. C., Ethé, C., Cadule, P., Aumont, O., Salas y Mélia, D., Voldoire, A., and Madec, G.: Skill assessment of three earth system models with common marine biogeochemistry, Clim. Dyn., 40, 2549–2573, https://doi.org/10.1007/s00382-012-1362-8, 2013.

Solan, M., Archambault, P., Renaud, P. E., and März, C.: The changing Arctic Ocean: consequences for biological communities, biogeochemical processes and ecosystem functioning, Philos. Trans. R. Soc. Math. Phys. Eng. Sci., 378, 20200266, https://doi.org/10.1098/rsta.2020.0266, 2020.

Deleted: Skákala, J., Bruggeman, J., Brewin, R. J. W., Ford, D. A., and Ciavatta, S.: Improved Representation of Underwater Light Field and Its Impact on Ecosystem Dynamics: A Study in the North Sea, J. Geophys. Res. Oceans, 125, https://doi.org/10.1029/2020JC016122, 2020.
Snowden, D., Tsontos, V. M., Handegard, N. O., Zarate, M., O' Brien, K., Casey, K. S., Smith, N., Sagen, H., Bailey, K., Lewis, M. N., and Arms, S. C.: Data Interoperability Between Elements of the Global Ocean Observing System, Front. Mar. Sci., 6, 442, https://doi.org/10.3389/fmars.2019.00442, 2019.
Sosik, H. M.: Characterizing seawater constituents from optical properties, Real-Time Coast. Obs. Syst. Ecosyst. Dyn. Harmful Algal Blooms Ed. Babin M Roesler CS Cullen JJ UNESCO, 281–329, 2008.

Steinacher, M., Joos, F., Frölicher, T. L., Bopp, L., Cadule, P., Cocco, V., Doney, S. C., Gehlen, M., Lindsay, K., Moore, J. K., Schneider, B., and Segschneider, J.: Projected 21st century decrease in marine productivity: a multi-model analysis, Biogeosciences, 7, 979–1005, https://doi.org/10.5194/bg-7-979-2010, 2010.

Stow, C. A., Jolliff, J., McGillicuddy, D. J., Doney, S. C., Allen, J. I., Friedrichs, M. A. M., Rose, K. A., and Wallhead, P.: Skill assessment for coupled biological/physical models of marine systems, J. Mar. Syst., 76, 4–15, https://doi.org/10.1016/j.jmarsys.2008.03.011, 2009.

Stramma, L., Johnson, G. C., Sprintall, J., and Mohrholz, V.: Expanding Oxygen-Minimum Zones in the Tropical Oceans, Science, 320, 655–658, https://doi.org/10.1126/science.1153847, 2008.

Tagliabue, A., Bopp, L., Dutay, J.-C., Bowie, A. R., Chever, F., Jean-Baptiste, P., Bucciarelli, E., Lannuzel, D., Remenyi, T., Sarthou, G., Aumont, O., Gehlen, M., and Jeandel, C.: Hydrothermal contribution to the oceanic dissolved iron inventory, Nat. Geosci., 3, 252–256, https://doi.org/10.1038/ngeo818, 2010.

Terzić, E., Lazzari, P., Organelli, E., Solidoro, C., Salon, S., D'Ortenzio, F., and Conan, P.: Merging bio-optical data from Biogeochemical-Argo floats and models in marine biogeochemistry, Biogeosciences, 16, 2527–2542, https://doi.org/10.5194/bg-16-2527-2019, 2019.

Deleted: Taylor, K. E.: Summarizing multiple aspects of model performance in a single diagram, J. Geophys. Res. Atmospheres, 106, 7183–7192, https://doi.org/10.1029/2000JD900719, 2001.
Teruzzi, A., Dobricic, S., Solidoro, C., and Cossarini, G.: A 3-D variational assimilation scheme in coupled transport-biogeochemical models: Forecast of Mediterranean biogeochemical properties: 3D-VAR IN BIOGEOCHEMICAL MODELS, J. Geophys. Res. Oceans, 119, 200–217, https://doi.org/10.1002/2013JC009277, 2014.

Thierry, V. and Bittig, H.: Argo quality control manual for dissolved oxygen concentration, 2018.

Thierry, V., Bittig, H., Gilbert, D., Kobayashi, T., Kanako, S., and Schmid, C.: Processing Argo oxygen data at the DAC level, Ifremer, https://doi.org/10.13155/39795, 2018.

Tuan Pham, D., Verron, J., and Christine Roubaud, M.: A singular evolutive extended Kalman filter for data assimilation in oceanography, J. Mar. Syst., 16, 323–340, https://doi.org/10.1016/S0924-7963(97)00109-7, 1998.

Tukey, J. W.: Exploratory Data Analysis, Addison-Wesley Publishing Company, 714 pp., 1977.

Ward, B. A., Friedrichs, M. A. M., Anderson, T. R., and Oschlies, A.: Parameter optimisation techniques and the problem of underdetermination in marine biogeochemical models, J. Mar. Syst., 81, 34–43, https://doi.org/10.1016/j.jmarsys.2009.12.005, 2010.

Westberry, T. K., Schultz, P., Behrenfeld, M. J., Dunne, J. P., Hiscock, M. R., Maritorena, S., Sarmiento, J. L., and Siegel, D. A.: Annual cycles of phytoplankton biomass in the subarctic Atlantic and Pacific Ocean, Glob. Biogeochem. Cycles, 30, 175–190, https://doi.org/10.1002/2015GB005276, 2016.

Williams, R. G. and Follows, M. J.: Ocean dynamics and the carbon cycle: Principles and mechanisms, Cambridge University Press, 2011.

Wong, Keeley, Robert, Carval, Thierry, and Argo Data Management Team,: Argo Quality Control Manual for CTD and Trajectory Data, https://doi.org/10.13155/33951, 2015.

Deleted: Vichi, M., Lovato, T., Lazzari, P., Cossarini, G., Gutierrez, E., Mattia, G., Masina, S., McKiver, W. J., Pinardi, N., and Solidoro, C.: The Biogeochemical Flux Model (BFM): Equation Description and User Manual, BFM version 5.1, BFM Report series N. 1, Release 1.1, July 2015, Bologna, Italy, 104pp, 2015.
Wanninkhof, R.: Relationship between wind speed and gas exchange over the ocean revisited: Gas exchange and wind speed over the ocean, Limnol. Oceanogr. Methods, 12, 351–362, https://doi.org/10.4319/lom.2014.12.351, 2014.

Deleted: Yang, B., Fox, J., Behrenfeld, M. J., Boss, E. S., Haëntjens, N., Halsey, K. H., Emerson, S. R., and Doney, S. C.: In Situ Estimates of Net Primary Production in the Western North Atlantic With Argo Profiling Floats, J. Geophys. Res. Biogeosciences, 126, https://doi.org/10.1029/2020JG006116, 2021.

Page 2: [1] Deleted Alexandre Mignot 21/12/2022 18:32:00

Page 9: [2] Deleted Alexandre Mignot 21/12/2022 18:32:00

i.

Page 18: [3] Deleted Alexandre Mignot 21/12/2022 18:32:00

Page 18: [4] Deleted Alexandre Mignot 21/12/2022 18:32:00

Page 18: [5] Deleted Alexandre Mignot 21/12/2022 18:32:00

Page 18: [6] Deleted Alexandre Mignot 21/12/2022 18:32:00

Page 22: [7] Deleted Alexandre Mignot 21/12/2022 18:32:00

Page 23: [8] Deleted Alexandre Mignot 21/12/2022 18:32:00

Page 23: [9] Deleted Alexandre Mignot 21/12/2022 18:32:00

Page 24: [10] Deleted Alexandre Mignot 21/12/2022 18:32:00

Page 25: [11] Deleted Alexandre Mignot 21/12/2022 18:32:00

Page 31: [12] Deleted Alexandre Mignot 21/12/2022 18:32:00